Atmospheric
Measurement
Techniques

An intercomparison of HO₂ measurements by fluorescence assay by gas expansion and cavity ring-down spectroscopy within HIRAC (Highly Instrumented Reactor for Atmospheric Chemistry)

Lavinia Onel[1], **Alexander Brennan**[1], **Michele Gianella**[2], **Grace Ronnie**[1], **Ana Lawry Aguila**[2], **Gus Hancock**[2], **Lisa Whalley**[1,3], **Paul W. Seakins**[1,3], **Grant A. D. Ritchie**[2], and **Dwayne E. Heard**[1,3]

[1]School of Chemistry, University of Leeds, Leeds, LS2 9JT, UK
[2]Department of Chemistry, Physical and Theoretical Chemistry Laboratory, University of Oxford, Oxford, OX1 3QZ, UK
[3]National Centre for Atmospheric Science, University of Leeds, Leeds, LS2 9JT, UK

Correspondence: Lavinia Onel (chmlo@leeds.ac.uk), Paul W. Seakins (p.w.seakins@leeds.ac.uk), Grant A. D. Ritchie (grant.ritchie@chem.ox.ac.uk), and Dwayne E. Heard (d.e.heard@leeds.ac.uk)

Abstract. The HO₂ radical was monitored simultaneously using two independent techniques in the Leeds HIRAC (Highly Instrumented Reactor for Atmospheric Chemistry) atmospheric simulation chamber at room temperature and total pressures of 150 and 1000 mbar of synthetic air. In the first method, HO₂ was measured indirectly following sampling through a pinhole expansion to 3 mbar when sampling from 1000 mbar and to 1 mbar when sampling from 150 mbar. Subsequent addition of NO converted it to OH, which was detected via laser-induced fluorescence spectroscopy using the FAGE (fluorescence assay by gas expansion) technique. The FAGE method is used widely to measure HO₂ concentrations in the field and was calibrated using the 185 nm photolysis of water vapour in synthetic air with a limit of detection at 1000 mbar of 1.6×10^6 molecule cm^{-3} for an averaging time of 30 s. In the second method, HO₂ was measured directly and absolutely without the need for calibration using cavity ring-down spectroscopy (CRDS), with the optical path across the entire ~ 1.4 m width of the chamber, with excitation of the first O-H overtone at 1506.43 nm using a diode laser and with a sensitivity determined from Allan deviation plots of 3.0×10^8 and 1.5×10^9 molecule cm^{-3} at 150 and 1000 mbar respectively, for an averaging period of 30 s. HO₂ was generated in HIRAC by the photolysis of Cl₂ using black lamps in the presence of methanol in synthetic air and was monitored by FAGE and CRDS for ~ 5–10 min periods with the lamps on and also during the HO₂ decay after the lamps were switched off. At 1000 mbar total pressure the correlation plot of [HO₂]$_{FAGE}$ versus [HO₂]$_{CRDS}$ gave an average gradient of 0.84 ± 0.08 for HO₂ concentrations in the range ~ 4–100×10^9 molecule cm^{-3}, while at 150 mbar total pressure the corresponding gradient was 0.90 ± 0.12 on average for HO₂ concentrations in the range ~ 6–750×10^8 molecule cm^{-3}.

For the period after the lamps were switched off, the second-order decay of the HO₂ FAGE signal via its self-reaction was used to calculate the FAGE calibration constant for both 150 and 1000 mbar total pressure. This enabled a calibration of the FAGE method at 150 mbar, an independent measurement of the FAGE calibration at 1000 mbar and an independent determination of the HO₂ cross section at 1506.43 nm, σ_{HO_2}, at both pressures. For CRDS, the HO₂ concentration obtained using σ_{HO_2}, determined using previous reported spectral data for HO₂, and the kinetic decay of HO₂ method agreed to within 20 and 12 % at 150 and 1000 mbar respectively. For the FAGE method a very good agreement (difference within 8 %) has been obtained at 1000 mbar between the water vapour calibration method and the kinetic decay of the HO₂ fluorescence signal method. This is the first intercomparison of HO₂ between the FAGE and CRDS methods, and the good agreement between HO₂ concentrations measured using the indirect FAGE method and the direct CRDS method provides validation for the FAGE method, which is used widely for field measurements of HO₂ in the atmosphere.

1 Introduction

The hydroperoxy radical, HO$_2$, plays a central role in the chemistry of the atmosphere (Levy, 1971) and is a significant reactive species in several media such as hydrocarbon combustion (Zador et al., 2011; Blocquet et al., 2013; Djehiche et al., 2014), atmospheric pressure plasmas (Gianella et al., 2016) and dielectric barrier discharges used to remove volatile organic compounds (VOCs) in air (Blin-Simiand et al., 2016). In the troposphere, HO$_2$ is generated directly by the reaction of a OH radical with CO in the presence of O$_2$ (Reaction R1) and indirectly by the oxidation of larger VOCs (Reactions R2–R4) (Lu et al., 2012).

$$OH + CO\,(+O_2) \rightarrow HO_2 + CO_2 \tag{R1}$$

$$RH + OH\,(+O_2) \rightarrow RO_2 + H_2O \text{ (R = organic group)} \tag{R2}$$

$$RO_2 + NO \rightarrow RO + NO_2 \tag{R3}$$

$$RO + O_2 \rightarrow R'O + HO_2 \tag{R4}$$
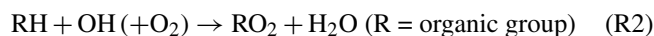
Ambient concentrations of HO$_2$ have been measured in a number of field campaigns and it has been found that maximum daytime concentrations are typically a few 10^8 molecule cm^{-3} (Heard and Pilling, 2003; Stone et al., 2012). With a typical lifetime in clean air of $\sim$1–2 min, HO$_2$ radicals participate in rapid chemical cycling at the heart of tropospheric oxidation; hence HO$_2$ is one of the best targets with which to compare chemical models with field data. HO$_2$ is converted back to OH through several different pathways. In unpolluted environments, its self-reaction and reaction with RO$_2$ are the major loss pathways for HO$_2$ via Reactions (R5)–(R7):

$$HO_2 + HO_2 \rightarrow H_2O_2 + O_2 \tag{R5}$$

$$HO_2 + HO_2 + M \rightarrow H_2O_2$$
$$+ O_2 + M\,(M = N_2 \text{ or } O_2) \tag{R6}$$

$$HO_2 + RO_2 \rightarrow ROOH + O_2. \tag{R7}$$
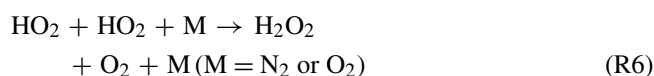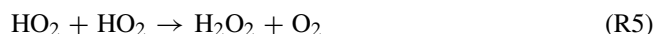
The reaction of HO$_2$ with NO dominates HO$_2$ loss in anthropogenically influenced environments and constitutes the main tropospheric in situ source of O$_3$ by Reactions (R8)–(R10).

$$HO_2 + NO \rightarrow OH + NO_2 \tag{R8}$$

$$NO_2 + h\nu\,(\lambda < 420\,\text{nm}) \rightarrow NO + O(^3P) \tag{R9}$$

$$O(^3P) + O_2 + M \rightarrow O_3 + M. \tag{R10}$$
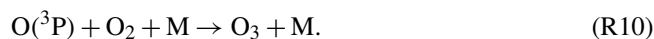
In the marine boundary layer the reaction of HO$_2$ with halogen oxides, XO (X = Br, I), is also an important OH regeneration reaction (Bloss et al., 2005):

$$HO_2 + XO \rightarrow HOX + O_2 \tag{R11}$$

$$HOX + h\nu \rightarrow OH + X. \tag{R12}$$

In addition, OH can be reformed from HO$_2$ via the relatively slow reaction with ozone:

$$HO_2 + O_3 \rightarrow OH + 2O_2. \tag{R13}$$

Because of its importance in various environments, HO$_2$ has been measured in laboratory experiments by a variety of spectroscopic methods. Early laboratory work studying the kinetics of HO$_2$ reactions used UV absorption near 220 nm to monitor HO$_2$ with detection limits of $\sim 6 \times 10^{11}$ molecule cm^{-3} (Kircher and Sander, 1984). The absorption spectrum of HO$_2$ in this region is broad, structureless and often overlapped by other species present in the system, such as RO$_2$ radicals and H$_2$O$_2$ produced by the HO$_2$ self-reaction (Reactions R5–R6); hence UV absorption spectroscopy is a relatively unselective technique. As the HO$_2$ absorption spectrum in the infrared (IR) is more structured than in the UV region, the selectivity of the IR absorption methods is higher. Although the near-IR range offers weaker absorption bands than the fundamental vibrational bands in the mid-IR region (Yamada et al., 1983; Zahniser and Stanton, 1984), near-IR lasers, detectors and optical components offer an improved performance over those in the mid-IR. Therefore, more recent advances in the direct detection of HO$_2$ have been made by the development of absorption techniques in the near IR, typically using diode laser absorption via the first vibrational overtone of the O–H stretch to monitor HO$_2$ by cavity absorption methods (Djehiche et al., 2011, 2014; Bell et al., 2012; Gianella et al., 2016) or conventional multi-pass/long-pass absorption spectroscopy (Tang et al., 2010), sometimes in combination with wavelength modulation spectroscopy (Taatjes and Oh, 1997; Christensen et al., 2004) or two-tone frequency modulation spectroscopy (Schocker et al., 2007; DeSain et al., 2003). The use of methods such as frequency modulation and intracavity absorption improves sensitivity, with typical detection limits in the range $\sim 10^9$–10^{11} molecule cm^{-3}. A recent addition to the spectroscopic techniques used for HO$_2$ detection in laboratory is mid-IR Faraday rotation spectroscopy, which has been employed for in situ measurements of HO$_2$ at atmospheric pressure in combustion studies using dimethyl ether to obtain a 1σ concentration detection limit of 0.1 ppmv (1.15×10^{12} molecule cm^{-3} at 623 K) (Brumfield et al., 2013; Kurimoto et al., 2015). While allowing a broad range of applications for spectroscopic and kinetic applications, these detection limits do not allow for the detection of HO$_2$ under atmospheric conditions where concentrations are typically around 10^8 molecule cm^{-3} (Heard and Pilling, 2003).

Cavity ring-down spectroscopy (CRDS) using the OH overtone vibrational band (2,0,0)–(0,0,0) of the ground electronic state $\widetilde{X}^2A''$ (the $2\nu_1$ band is centred at 6648.9 cm^{-1} i.e. $\sim$ 1504 nm; Thiebaud et al., 2007) of HO$_2$ has been applied in a number of studies to detect HO$_2$ at reduced pressure (Liu et al., 2008; Djehiche et al., 2014). The CRDS technique (O'Keefe and Deacon, 1988; Wheeler et al., 1998; Brown, 2003) is well established and consists of trapping a laser beam within a high-finesse optical resonator formed by two highly reflective dielectric mirrors. If the laser frequency matches one of the cavity resonance frequencies, op-

tical power within the resonator quickly builds up, and a fraction of the circulating power leaks out through one mirror. A photodetector located at the back of this mirror measures the exponential decay in the light intensity (ring-down) with a time constant that is a measure of the cavity losses. If an absorbing gas is introduced into the cavity, the ring-down time will decrease due to the additional absorption loss. The concentration of the absorbing species, [A], is related to the difference in ring-down times via (O'Keefe and Deacon, 1988)

$$[A] = \frac{1}{\sigma c} \left(\frac{1}{\tau} - \frac{1}{\tau_0} \right), \qquad (1)$$

where σ is the absorption cross section of the species A, c is the velocity of light, and τ and τ_0 are the ring-down times in the presence and absence of the absorber.

Fittschen and co-workers have used the CRDS technique to perform time-resolved measurements of the HO$_2$ radicals generated by pulsed laser photolysis in a flow cell, to extract spectroscopic (Thiebaud and Fittschen, 2006; Ibrahim et al., 2007; Thiebaud et al., 2007; Parker et al., 2011; Assaf et al., 2017) and kinetic (Thiebaud and Fittschen, 2006; Morajkar et al., 2014) information. The majority of the experiments have been conducted at room temperature to provide absorption cross sections and spectral line strengths at 50 Torr of He (Thiebaud et al., 2007; Parker et al., 2011) and air-broadening coefficients of the spectral lines (Ibrahim et al., 2007) (by using pressures between 7 and 160 Torr) for HO$_2$ in the $2\nu_1$ band. The most significant absorption feature in the wavelength range 6604–6696 cm^{-1} has been found at 6638.20 cm^{-1} (i.e. 1506.43 nm), with a Doppler-limited peak cross section of $\sigma_D = 4.2 \times 10^{-19}$ cm^2 molecule^{-1} (no errors quoted), in very good agreement with the conventional multi-pass study performed by Tang et al. (2010), which reports $\sigma_D = (4.3 \pm 1.1) \times 10^{-19}$ cm^2 molecule^{-1} at the same wave number. Fittschen and co-workers calculated a minimum detectable concentration of HO$_2$ of 3.2×10^9 molecule cm^{-3} for detection at 6638.20 cm^{-1} with a 1 Hz detection bandwidth (1 s integration time) (Thiebaud et al., 2008).

Despite its significance, at present HO$_2$ is not typically measured directly in the atmosphere. Previous direct measurements of HO$_2$ were performed by the matrix isolation electron spin resonance (MIESR) technique (Mihelcic et al., 1978), but this method has been retired and was characterised by long averaging times (30 min; Fuchs et al., 2009). However, recently chemical ionisation mass spectrometry (CIMS) employing Br$^-$ as a reagent ion has been used for direct HO$_2$ measurements with a limit of detection of $\sim 1.7 \times 10^7$ molecule cm^{-3} for a 1 min integration time (Sanchez et al., 2016). Laser-induced fluorescence (LIF) at low pressure, known as fluorescence assay by gas expansion (FAGE) (Heard and Pilling, 2003; Stone et al., 2012), is most commonly used for the measurements of OH and HO$_2$. However, HO$_2$ is not detected directly, rather it is converted to OH by reaction with added NO (Reaction R8) followed by OH on-resonance LIF at 308 nm (Hard et al., 1992).

FAGE is a sensitive technique with a typical detection limit for HO$_2$ of $(5–10) \times 10^5$ molecule cm^{-3}, depending on the individual instrument, averaging time and the desired signal-to-noise ratio (Stone et al., 2012). Another indirect method uses CIMS to determine the sum of HO$_2$ and the organic peroxy radicals (RO$_2$), $[HO_2] + \sum_i [RO_{2,i}]$, or separately $[HO_2]$, depending on the flows of the NO and SO$_2$ reagents (Hanke et al., 2002; Edwards et al., 2003). A typical detection limit for the indirect CIMS (sometimes referred to as per-CIMS or ROXMAS) method is 1×10^7 molecule cm^{-3} for 15 s averaging time (Hanke et al., 2002; Edwards et al., 2003). The HO$_2$ concentrations at an urban site have also been recently derived from observations of HO$_2$NO$_2$ by using CIMS with I$^- \cdot$(H$_2$O)$_n$ as a reagent ion combined with measurements of NO$_2$ by cavity-attenuated phase shift spectroscopy (Chen et al., 2017). The peroxy radical chemical amplifier (PERCA) method has been used for many years to determine the sum $[HO_2] + \sum_i [RO_{2,i}]$ by using NO and CO to generate NO$_2$, which is amplified by a chain reaction and subsequently measured through a range of methods, such as luminol fluorescence, LIF or cavity absorption methods, with typical detection limits in the range of $1–2.5 \times 10^7$ molecule cm^{-3} in a 1 min time period (Cantrell and Stedman, 1982; Cantrell et al., 1984; Green et al., 2006; Miyazaki et al., 2010; Chen et al., 2016). A recently developed method is RO$_x$LIF, which is an extension of FAGE, enabling HO$_2$ and $\sum_i [RO_{2,i}]$ to be measured separately (Fuchs et al., 2008) and with good sensitivity ($\sim 2.5 \times 10^6$ molecule cm^{-3} detection limit in 1 min). The concentration of the initial HO$_2$ is determined by subtracting the separate direct measurement of [OH] from the indirect measurement of $[HO_x] = [OH] + [HO_2]$ by converting HO$_x$ to HO$_2$ through addition of CO followed by the HO$_2$ conversion into OH in the FAGE detection chamber.

While FAGE has the appropriate sensitivity and time resolution for atmospheric monitoring, there are two issues that could potentially cause systematic errors with this technique. First, FAGE is not an absolute method and hence requires a calibration which may lead to a source of error. Secondly, it is not a direct technique but requires chemical conversion to another species, OH, which is subsequently detected by LIF spectroscopy and hence may be subject to additional uncertainties associated with the conversion, i.e. could be prone to interferences arising from the conversion of species other than HO$_2$ to OH. One known interference of this type is the conversion of beta-hydroxyalkyl peroxy radicals (Fuchs et al., 2011; Whalley et al., 2013). For calibration, the most common method used to generate accurate known concentrations of OH and HO$_2$ uses the photolysis of water vapour

at 184.9 nm in zero air employing a mercury Pen-Ray lamp:

$$H_2O \xrightarrow{184.9\,nm} OH + H \tag{R14}$$

$$H + O_2 + M \rightarrow HO_2 + M. \tag{R15}$$
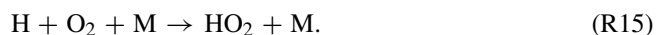
The water photolysis method has been used for many years for the calibration of FAGE instruments (Heard and Pilling, 2003; Stone et al., 2012). The reliability of the method has been confirmed by intercomparisons with alternative methods of calibration for OH and HO$_2$. For HO$_2$, the kinetics of the second-order decay of HO$_2$ via its self-reaction has been observed in HIRAC (Highly Instrumented Reactor for Atmospheric Chemistry) to obtain a FAGE calibration factor in good agreement with the one determined by using the water photolysis method for a pressure in the fluorescence detection cell between 1.4 and 3.8 mbar (Winiberg et al., 2015).

Intercomparisons between different HO$_2$ instruments have been used to probe the susceptibility of instruments towards any bias, for example via the calibration methodology used and potential interferences. In 2005, three FAGE instruments measured HO$_2$ during the HO$_x$Comp campaign, showing variable agreement with correlation slopes between 0.69 and 1.26 in the SAPHIR (Simulation of Atmospheric PHoto-chemistry In a large Reaction) chamber and sometimes worse correlations in ambient air (Fuchs et al., 2010). Agreement while detecting HO$_2$ in the same location for various designs of the FAGE technique increases the confidence in the use of the FAGE method, but such intercomparisons are rare. A field intercomparison between FAGE and CIMS measurements of HO$_2$ gave agreement within 40 % (Ren et al., 2003), while a subsequent intercomparison between RO$_x$LIF and MIESR techniques for HO$_2$ in the SAPHIR chamber resulted in a very good agreement, with correlation slopes of 0.98 ± 0.08 (1σ) (Fuchs et al., 2009).

This paper reports the first intercomparison between FAGE and CRDS measurements of HO$_2$. The experiments have been performed at room temperature and two different pressures: 150 and 1000 mbar within the HIRAC atmospheric simulation chamber (Glowacki et al., 2007). For measurements at 1000 mbar, FAGE was calibrated using the conventional water vapour photolysis method, while at 150 mbar the FAGE calibration constant was determined by studying the kinetics of HO$_2$ via its self-reaction, where the time constant of the second-order decay depends on the absolute, initial concentration of HO$_2$, [HO$_2$]$_0$. The CRDS technique was chosen to confirm the HO$_2$ measurements by the FAGE method as CRDS is a direct absorption method that does not require the chemical conversion of HO$_2$ to another species. Reported here are the first CRDS measurements of HO$_2$ carried out in an atmospheric simulation chamber. The newly constructed CRDS spectrometer consists of a high-finesse linear optical cavity set up across the chamber for the in situ direct HO$_2$ detection over a distance of ~ 1.4 m between two highly reflective dielectric mirrors ($R > 0.9999$; typical ring-down time $\tau = 230\,\mu s$), which results in ~ 70 km effective

absorption path length. The use of a homogeneously mixed chamber allowed the same [HO$_2$] to be sampled by the two techniques. A further advantage of the use of HIRAC is that the experiments can be performed under controlled conditions which produce approximately constant [HO$_2$] at different levels and, in addition, can generate HO$_2$ temporal decays by turning off the UV lamps employed for the generation of the radicals in the chamber. The CRDS spectrometer used diode laser light at 1506.43 nm (vacuum wavelength, corresponding to 6638.2 cm^{-1}) to probe HO$_2$ at its peak absorption in the $2\nu_1$ band. The HO$_2$ cross sections at 1506.43 nm, σ_{HO_2}, at 150 and 1000 mbar are estimated using the reported HO$_2$ spectra and pressure-broadening coefficients for the transitions contributing to σ_{HO_2} (Thiebaud et al., 2007) and are compared with values obtained by analysing the second-order temporal decays of HO$_2$ monitored by CRDS and FAGE.

2 Experimental

2.1 HO$_2$ generation in HIRAC

Experiments were conducted in HIRAC, at 295 K and in 150 and 1000 mbar of synthetic air obtained by mixing high-purity oxygen (BOC, > 99.999 %) and nitrogen (BOC, > 99.998 %) in the ratio of O$_2$: N$_2$ = 1 : 4. HIRAC is a stainless steel cylinder with internal dimensions of 2.0 m length and 1.2 m diameter (Fig. 2a below), which was built with a number of flanges to allow for easy coupling of equipment and has been described in detail previously (Glowacki et al., 2007). Thorough mixing of the gas mixtures was achieved by four low-vibration circulation fans mounted in pairs at each end of the chamber. Methanol (Sigma Aldrich, HPLC grade, ≥ 99.9 %, (0.7–1.4) $\times 10^{14}$ molecule cm^{-3} in the experiments at 150 mbar and (0.8–2.0) $\times 10^{14}$ molecule cm^{-3} in the experiments at 1000 mbar) and molecular chlorine (Sigma Aldrich, ≥ 99.5 %, 7×10^{12}–2.1 $\times 10^{14}$ molecule cm^{-3} in the experiments at 150 mbar and (0.4–1.6) $\times 10^{14}$ molecule cm^{-3} in the experiments at 1000 mbar) were delivered to the chamber. The chemistry generating HO$_2$ was initiated by the photolysis of Cl$_2$ using eight UV black lamps (Phillips, TL-D36W/BLB, $\lambda = 350$–400 nm) housed in quartz tubes mounted radially inside the reactive volume (aligned parallel to the chamber longitudinal axis):

$$Cl_2 \xrightarrow{h\nu} Cl + Cl \tag{R16}$$

$$CH_3OH + Cl \rightarrow CH_2OH + HCl \tag{R17}$$

$$CH_2OH + O_2 \rightarrow HO_2 + CH_2O. \tag{R18}$$
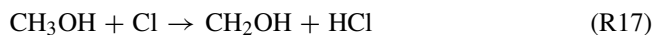
Two kinds of intercomparison studies have been performed: experiments in which the UV lamps were turned on for 5–10 min to generate a slowly changing [HO$_2$] and then off to follow the HO$_2$ decay (Sect. 3.5) and experiments where the

lamps were alternately turned on for 2–3 min and then off for ~ 3 min to generate a series of three HO_2 temporal decays followed by regeneration of the HO_2. Figures S7 and S8 in the Supplement are examples of the series of HO_2 decays measured at the two pressures.

2.2 FAGE instrument

Full details on the HIRAC FAGE instrument can be found in previous publications (Winiberg et al., 2015, 2016; Onel et al., 2017). In the FAGE method, gas was sampled from the HIRAC chamber via a 50 mm diameter sampling inlet into a reduced-pressure fluorescence cell where OH (either present in the HIRAC chamber or converted from HO_2) was detected by LIF. Although capable of simultaneously determining OH and HO_2, only data from the HO_2 measurements are described here.

In order to detect the HO_2 radicals generated within HIRAC, the FAGE instrument was coupled to the chamber through a custom-made ISO-K160 flange to sample the gas at ~ 230 mm from the chamber wall (Fig. 2a in Sect. 2.4). Under typical operating conditions, air was sampled at ~ 3 slm through a 1.0 mm diameter pinhole nozzle and passed down the inlet (length 280 mm, 50 mm diameter, although the length was varied in some experiments, see below) into the OH detection axis maintained at low pressure using a high-capacity rotary pump-backed roots blower pumping system (Leybold, trivac D40B and ruvac WAU251). Concentrations of HO_2 were measured simultaneously in a second detection axis ~ 300 mm downstream of the OH detection axis (internal pressure $= (3.24 \pm 0.20)$ mbar when sampling from 1000 mbar). High-purity NO (BOC, N2.5 nitric oxide) was added ~ 25 mm before the HO_2 detection axis into the centre of the FAGE cell in the direction of gas flow through 1/8-inch diameter stainless steel tubing at a rate of 2.5 sccm (Brooks 5850S), converting a fraction of HO_2 to OH. LIF with excitation at 308 nm (using the Q1(2) rotational line of the $A^2\Sigma^+ (v'=0) \leftarrow X^2\Pi_i (v''=0)$ transition) was used to probe the OH radicals directly, and the resulting fluorescence was collected after passing through an interference filter $(308.8 \pm 5.0$ nm). Laser light was generated using a pulsed Nd:YAG (JDSU Q201HD) pumped dye laser (SIRAH Credo-Dye-N) operating at 5 kHz pulse repetition frequency and was delivered via fibre optics to the fluorescence and reference cells. The laser power entering the HO_2 fluorescence cell was typically 3–5 mW. A small portion of the laser light was directed into a reference cell where high concentrations of OH were generated from the thermal dissociation of water. The use of a reference cell maintained the laser at the optimum wavelength and the laser power reaching the reference cell was monitored to allow normalisation of the fluorescence signal to fluctuations in laser power.

2.3 FAGE calibration for HO₂

2.3.1 Calibration at atmospheric pressure – H₂O vapour photolysis

As described above and detailed in Winiberg et al. (2015), the photolysis of water vapour at 184.9 nm is used to generate known concentrations of OH and HO_2. A humidified flow of zero air (40 SLM, BOC, BTCA 178) was passed into a square cross-section flow tube with [H_2O] measured using a dew-point hygrometer (CR4, Buck Research Instruments). The collimated 184.9 nm output of a mercury lamp (LOT-Oriel, Pen-Ray) was introduced to the end of the flow tube to photolyse the water. The gas output from the flow tube was directed towards the FAGE sampling inlet, where overfilling of the FAGE sampling inlet ensured no ingress of ambient air. A range of HO_x concentrations was produced by changing the lamp current.

The HO_x concentrations are given by

$$[OH] = [HO_2] = [H_2O]\sigma_{H_2O,\,184.9\,nm}\Phi_{H_2O}F_{184.9\,nm}\Delta t, \quad (2)$$

where $\sigma_{H_2O,\,184.9\,nm}$ is the photolysis cross section of water at 184.9 nm, Φ_{OH} is the quantum yield for OH formation (unity), $F_{184.9\,nm}$ is the photon flux and Δt is the photolysis time. The photolysis cross section and quantum yield are well known and the product $F_{184.9\,nm}\Delta t$ is determined by N_2O actinometry (Edwards et al., 2003). An example of a calibration plot is shown in the Supplement (Fig. S1). The resultant average calibration constant was

$$C_{HO_2} = (2.6 \pm 0.4) \times 10^{-7}\ \text{counts}\,cm^3\,molecule^{-1}\,s^{-1}\,mW^{-1},$$

where C_{HO_2} is defined by $S_{HO_2} = C_{HO_2}[HO_2]$ and the error is a combination of systematic and statistical uncertainties at the 1σ level. The resulting limit of detection (LOD) for a signal-to-noise ratio (S/N) of 2 and 2 min averaging was LOD $= 7.8 \times 10^5$ molecule cm^{-3}. The value of the calibration constant is in very good agreement with the value obtained by using the kinetic decay method based on the determination of a HO_2 second-order recombination (Sect. S2 in the Supplement and Winiberg et al., 2015) at 1000 mbar, which gives $C_{HO_2} = (2.4 \pm 0.5) \times 10^{-7}$ counts cm^3 molecule^{-1} s^{-1} mW^{-1}. The principle behind the kinetic method of calibration is that the time constant of the second-order decay of HO_2 in the self-reaction is dependent upon its initial concentration, and hence its analysis offers an alternative way to calibrate the signal. Winiberg et al. (2015) have shown that C_{HO_2} is relatively invariant between the high water vapour concentrations of the flow tube calibration method ([H_2O] $\sim 7 \times 10^{16}$ molecule cm^{-3}) and the relatively dry conditions in HIRAC ([H_2O] $\sim 10^{13}$–10^{14} molecule cm^{-3}) for the HO_2 recombination method. Therefore, the average value of these methods is $\bar{C}_{HO_2,\,1000\,mbar} = (2.5 \pm 0.5) \times 10^{-7}$ counts cm^3 molecule^{-1} s^{-1} mW^{-1}.

2.3.2 Calibration at 150 mbar – kinetics of the HO$_2$ temporal decay

The kinetics of the temporal decay of HO$_2$ has been used as the calibration method of FAGE sampling from HIRAC at 150 mbar (fluorescence cell pressure $= (1.0 \pm 0.1)$ mbar). This method was previously validated for HO$_2$ in HIRAC, where the FAGE calibration constant, C_{HO_2}, obtained from the analysis of the temporal decay of HO$_2$ (generated by the photolysis of HCHO, then the chamber lamps switched off) agreed with C_{HO_2} from the conventional water vapour photolysis method for a range of pressures in the fluorescence detection cell, 1.3–3.9 mbar (Winiberg et al., 2015). The variation of C_{HO_2} is small and linear and therefore the uncertainties associated with the short extrapolation for the internal cell pressure of 1.3 to 1.0 mbar are small.

In order to generate the second-order decays the chamber photolysis lamps were turned off. The HO$_2$ was consumed by the bimolecular and termolecular self-reactions (Reactions R5–R6) and removed by the first-order wall loss. In order to investigate whether HO$_2$ removal by the wall loss is significant, the experimental data were fitted by two different equations. Equation (3) assumes that the loss of HO$_2$ is due entirely to the overall self-reaction (Reactions R5–R6), i.e. without taking into account the wall loss of HO$_2$.

$$(S_{HO_2})_t = \left(\frac{1}{(S_{HO_2})_0} + \frac{2 \cdot k_{\text{self-r.}} t}{C_{HO_2}} \right)^{-1}, \qquad (3)$$

where $(S_{HO_2})_t$ is the fluorescence signal at reaction time t, $(S_{HO_2})_0$ is the signal at time $t = 0$ when the lamps were switched off and $k_{\text{self-r.}}$ is the overall HO$_2$ self-reaction rate coefficient. Equation (4) includes the HO$_2$ wall loss as a first-order process:

$$(S_{HO_2})_t = \left(\left(\frac{1}{(S_{HO_2})_0} + \frac{2 \cdot k_{\text{self-r.}}}{k_{\text{loss}} \cdot C_{HO_2}} \right) \right.$$
$$\left. \times \exp(k_{\text{loss}}t) - \left(\frac{2 \cdot k_{\text{self-r.}}}{k_{\text{loss}} \cdot C_{HO_2}} \right) \right)^{-1}, \qquad (4)$$

where k_{loss} is the rate coefficient describing the HO$_2$ wall loss.

Figure 1 shows an example of the experimental decay of S_{HO_2} with data averaged over 0.1 s (500 laser pulses) and the fits given by Eqs. (3) and (4) above fixing $k_{\text{self-r.}}$ to 1.79×10^{-12} cm^3 molecule^{-1} s^{-1}, according to the IUPAC recommendation (Atkinson et al., 2004), and with C_{HO_2} and k_{loss} floated. It is clear that wall losses must be included in order to provide a good fit to the data, especially at later times ($r^2 = 0.99$). This result is in agreement with previous HO$_2$ calibrations where Eq. (4) was applied to analyse the kinetics of the HO$_2$ decays generated in HIRAC (Winiberg et al., 2015). Therefore, Eq. (4) has been chosen to fit the experimental data. Nine HO$_2$ decays were analysed, which yielded an average value of
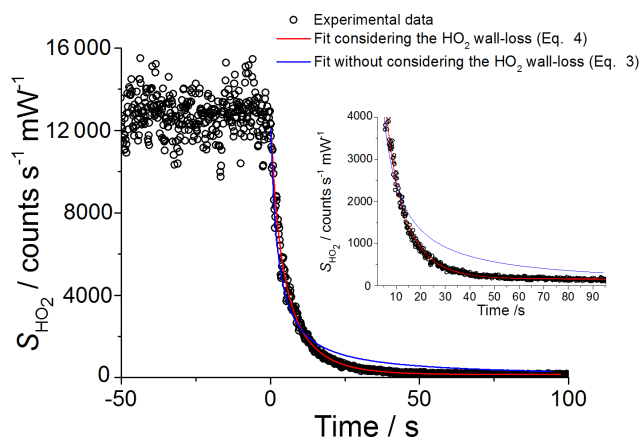
Figure 1. An example of temporal decay of the normalised FAGE HO$_2$ signal with 0.1 s time resolution recorded at 295 K and 150 mbar mixture of N$_2$: O$_2$ = 4 : 1 using Cl$_2$/CH$_3$OH and the black lamps (details given in the main text): [Cl$_2$]$_0 \sim 3 \times 10^{13}$ molecule cm^{-3} and [CH$_3$OH]$_0 \sim 5 \times 10^{13}$ molecule cm^{-3}. At time zero the photolysis lamps were turned off. Fitting Eq. (4) to this example trace (red line) gave $C_{HO_2} = (2.45 \pm 0.06) \times 10^{-7}$ counts cm^3 molecule^{-1} s^{-1} mW^{-1} ($r^2 = 0.99$), while fitting Eq. (3) to the data (blue line) led to $C_{HO_2} = (1.06 \pm 0.02) \times 10^{-7}$ counts cm^3 molecule^{-1} s^{-1} mW^{-1} ($r^2 = 0.95$) – statistical errors at 1σ level. The inset shows the fit to the data using the two equations at later times. Note that the most significant source of the signal noise is the shot noise (Poisson noise), which grows with the number of photons counted by the detector.

$C_{HO_2} = (2.6 \pm 0.5) \times 10^{-7}$ counts cm^3 molecule^{-1} s^{-1} mW^{-1}. Therefore, $C_{HO_2,\,150\,mbar} \cong C_{HO_2,\,1000\,mbar}$ ($\bar{C}_{HO_2,\,1000\,mbar} = (2.5 \pm 0.5) \times 10^{-7}$ counts cm^3 molecule^{-1} s^{-1} mW^{-1}; Sect. 2.3.1), which agrees with the negligible change in C_{HO_2} with the decrease in the detection cell pressure found previously (Winiberg et al., 2015). The wall loss rate coefficient obtained from the fit, $k_{\text{loss}} = (0.09 \pm 0.02)$ s^{-1}, has overlapping error limits with the range of values reported previously for HO$_2$ in HIRAC, (0.03–0.07) s^{-1} (Winiberg et al., 2015).

2.3.3 FAGE measurements of HO$_2$ across the HIRAC diameter

In order to ensure that the point measurements of [HO$_2$] with FAGE and the CRDS measurements of the average [HO$_2$] across the width of the chamber (see Sect. 2.4) are comparable, investigations into any [HO$_2$] gradient across the ~ 600 mm radius of the chamber were performed. HO$_2$ was generated either from the photolysis of formaldehyde at 270–320 nm (lamps: Philips TL40W/12 RS) in air at 150 mbar, which produced HO$_2$ by the reaction of O$_2$ with the H atoms and the HCO radicals generated by CH$_2$O photolysis, or O$_3$ photolysis at 254 nm (lamps: GE G55T8/OH 7G) followed
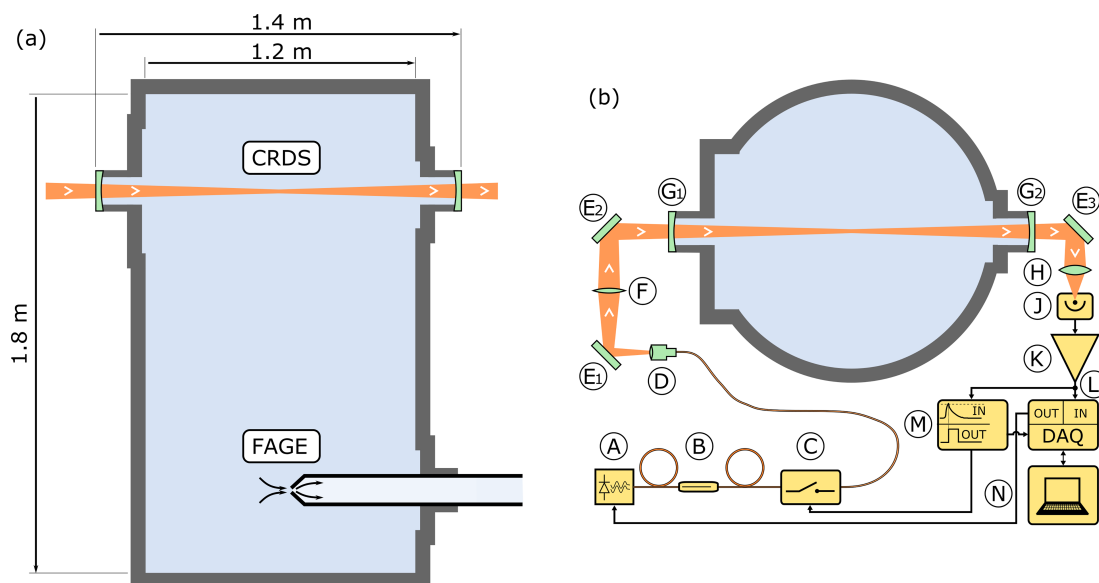
Figure 2. (a) Longitudinal (horizontal) section of HIRAC. The CRDS spectrometer probes the HO$_2$ concentration across the chamber's diameter, while the FAGE instrument samples the atmosphere in the chamber at one point. **(b)** Cross section of HIRAC. [A] Fibre-pigtailed DFB laser diode and mount, [B] inline optical isolator, [C] acousto-optic modulator (AOM), [D] adjustable fibre collimator, [E1]–[E3] silver mirrors, [F] $f = 250$ mm mode-matching lens, [G1]–[G2] high-reflectivity dielectric cavity mirrors, [H] $f = 30$ mm focusing lens, [J] InGaAs photodiode, [K] transimpedance amplifier, [L] data acquisition unit, [M] latched comparator circuitry, [N] laptop running LabVIEW for data processing and storing.

by the reaction of the O(^{1}D) generated with H$_2$O to produce OH and then by the reaction of OH with O$_3$ at 1000 mbar of air. An extended FAGE inlet of a length of ~ 520 mm was used to sample at separate locations up to 500 mm across HIRAC. At both pressures a constant [HO$_2$] was found (within the 10 % 1σ precision uncertainty of the measurement) at locations between ~ 100 and 500 mm from the wall, while [HO$_2$] gradually decreased between ~ 100 and 0 mm from the wall; the maximum ~ 16 % decrease occurred when the sampling pinhole was flush with the wall. This result is in good agreement with previous studies (Winiberg et al., 2015) and means that the point measurements of the FAGE system can readily be compared with the CRDS results. In addition, investigations into the radiation field profile within HIRAC have been performed to show that the distribution of the light intensity varies by less than 15 % in ~ 75 % the chamber volume (Glowacki et al., 2007).

2.4 CRDS set-up

The CRDS spectrometer was set up across the HIRAC diameter as shown in Fig. 2. To probe HO$_2$, a diode laser beam at ~ 1506 nm is sent diametrically across the chamber (Fig. 2a). On either side there is a blank flange (ISO-K 500 on the injection side, ISO-K 160 on the detection side) onto which KF25 flanges have been welded so that a pair of home-made mirror mounts can be attached. A sketch of the cavity ring-down spectrometer is given in Fig. 2b. The $\lambda \sim 1.5$ μm distributed feedback (DFB) fibre pig-tailed diode

laser [A] (NTT Electronics, NLK1S5GAAA) is held in a butterfly laser diode mount (Thorlabs LM14S2). Current to the laser diode and the built-in thermoelectric element is provided by a Thorlabs ITC502 driver. The single-mode fibre is connected to an inline optical isolator [B] (Thorlabs IO-H-1505APC), an acousto-optic modulator [C] (AOM, Gooch & Housego Fibre-Q T-M040-0.5C8J-3-F2S) and an adjustable fibre collimation package [D] (Thorlabs CFC-8X-C). The AOM is powered by a 0.5 W 40 MHz radio-frequency driver (Gooch & Housego A35040-0.5W). The components [A], [B] and [C] lie on a small optical breadboard plate attached to HIRAC's support frame under the ISO-K 500 flange.

The free-space components [D], [E1], [E2] and [F] on the beam injection side (of the cavity) and [E3], [H] and [J] on the detection side are assembled with a Thorlabs 30 mm cage system, which in turn is supported by posts clamped onto HIRAC itself. This solution mitigates misalignment of the cavity axis relative to the beam axis under the effect of the mechanical deformation (pressure difference) of HIRAC and low vibrations caused by the chamber's circulating fans. After the fibre collimator [D], a protected silver mirror [E1] (Thorlabs PF10-03-P01) is followed by a $f = 250$ mm mode-matching lens [F] (Thorlabs LA1461-C) and a second identical mirror [E2]. The 1-inch diameter cavity mirrors [G1] and [G2] (Layertec, reflectivity: $R > 0.9999$, curvature radius: 1 m; the mode diameter varies from ~ 1 mm in the centre of the chamber to ~ 1.7 mm at the cavity mirrors) are housed in a pair of home-built mounts, which allow the mir-

rors to tilt slightly while maintaining a gas-tight seal. The mounts are both attached to KF25 flanges welded onto the ISO-K 500 flange on the beam injection side and onto a smaller ISO-K 160 flange on the detection side. The mirror [G1] can be moved by a few microns along the beam's axis by means of a piezoelectric transducer. The distance between the two mirrors is approximately 1.4 m. On the detection side, the mirror [E3] (Thorlabs PF10-03-P01) is followed by a $f = 30$ mm focusing lens [H] (Thorlabs LA1805-C) and an InGaAs photodiode [J] (Thorlabs DET10C/M).

A low-noise transimpedance amplifier [K] (FEMTO DLPCA-200) sends the photodiode signal to the data acquisition unit [L] (DAQ, National Instruments USB-6361) and to a home-made latched comparator [M] (trigger box). The comparator compares the photodiode signal with an adjustable threshold. When the signal crosses the threshold, the AOM is powered off (blocking the beam) and a trigger pulse is sent to the DAQ to start acquisition of the ring-down event. After a predefined duration (typically 5 ms), the AOM is powered back on and the system is ready for the next ring-down event. The digitised data are processed by a custom LabVIEW programme (National Instruments) running on a laptop [N]. The programme fits all acquired ring-down events with an exponential function and can run in two modes: fixed wavelength and scan. In fixed wavelength mode, the programme was set up to save all ring-down events as a function of time. A number of filters can be applied to the processed events to exclude outliers (caused for example by a dust particle passing through the beam) or false positives (when the acquisition is triggered by a transient noise spike), so that only legitimate ring-down events are taken into account. In scan mode, the wavelength of the laser is stepped (by changing the diode's temperature) each time a predefined number of ring-down events has been acquired and the mean ring-down time is determined as a function of wavelength. The laser emission wavelength has been calibrated using a wavemeter (Burleigh WA-1000). An example of the laser calibration plot (λ versus thermistor resistance) is shown in the Supplement (Fig. S2). In addition, the calibration has been confirmed by reproducing the well-known transmission spectrum of water vapour in the range ∼ 1506.1–1506.9 nm (Richard et al., 2012) at both 150 and 1000 mbar (Fig. S3 in the Supplement).

3 Results

3.1 HO$_2$ spectrum and comparison with literature

Figure 3 shows typical wavelength scans performed at the two HIRAC pressures. A higher spectral resolution was chosen for the measurement at 150 mbar (8×10^{-4} nm per point and averaged for 50 ring-down events per point) than for the spectral measurement at 1000 mbar (2×10^{-3} nm per point and averaged for 25 events per point), as at a lower pressure the HO$_2$ absorption spectrum is more structured, as shown in Fig. 3, owing to reduced pressure broadening. These
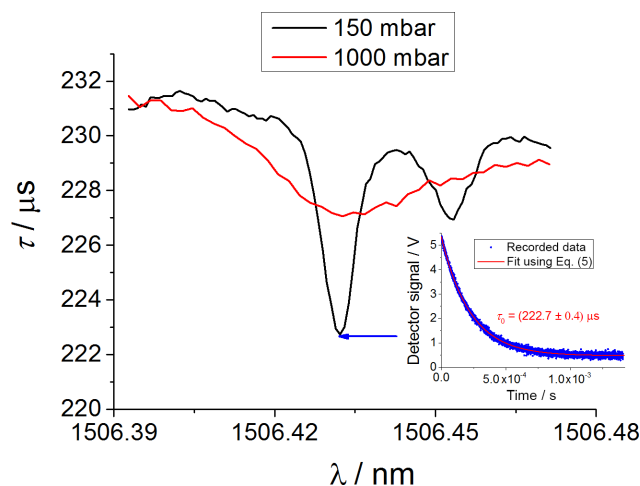
Figure 3. Typical laser scans of the ring-down time, τ, as a function of wavelength, recorded for a HIRAC pressure of 150 mbar (black line) and 1000 mbar (red line) mixture of N$_2$: O$_2 = 4$: 1 and 295 K. For the sake of clarity the measurement at 1000 mbar was rescaled by adding 18 μs to τ. HO$_2$ radicals were generated in the chamber using CH$_3$OH / Cl$_2$ / O$_2$ and black lamps: $[CH_3OH]_0 = 7 \times 10^{13}$ molecule cm^{-3} and $[Cl_2]_0 = 4 \times 10^{13}$ molecule cm^{-3} in the experiment at 150 mbar and $[CH_3OH]_0 = 2 \times 10^{14}$ molecule cm^{-3} and $[Cl_2]_0 = 2 \times 10^{14}$ molecule cm^{-3} in the experiment at 1000 mbar. The number of ring-down events averaged at each wavelength and the laser wavelength step were 50 events and 8×10^{-4} nm (150 mbar) and 25 events and 2×10^{-3} nm (1000 mbar). The inset shows the ring-down trace acquired at 1506.43 nm and 150 mbar and the fit by Eq. (5) to extract $\tau = (222.7 \pm 0.4)$ μs.

choices lead to recording times of ∼ 9 min at 150 mbar and 2–3 min at 1000 mbar. The maximum HO$_2$ absorption was recorded at 1506.43 nm (6638.20 cm^{-1}; Fig. 3), where the strongest HO$_2$ absorption line in the range ∼ 1493–1514 nm (∼ 6604–6696 cm^{-1}) of the first overtone of the OH stretch has been reported to lie at (Thiebaud et al., 2007). Therefore, the FAGE–CRDS intercomparison experiments were run at a fixed wavelength of 1506.43 nm. The spectral feature at 1506.43 nm consists of overlapping $^qQ_3(N)$ transitions with $N = 4$–9, each of which is doubled by spin-rotation splitting, as originally assigned by Taatjes and co-workers (DeSain et al., 2003) who observed the absorption spectrum of the HO$_2$ in the $2\nu_1$ band at ∼ 20 mbar of He. Next to the 1506.43 nm feature there is a weaker HO$_2$ absorption line at 1506.45 nm, which has been assigned to the spin-rotation split $^qP_0(6)$ transitions. As shown in Fig. 3, at 150 mbar there is little overlapping of the absorption lines, and the recorded features centred at 1506.43 nm and 1506.45 nm can be mainly attributed to the $^qQ_3(N)$ and $^qP_0(6)$ transitions respectively. In contrast, the laser scans performed at 1000 mbar of air showed a relatively broad spectral feature centred at 1506.43 nm as the air-broadening of the HO$_2$ absorption lines resulted in a significant overlap of the 1506.43 nm line with the 1506.45 nm
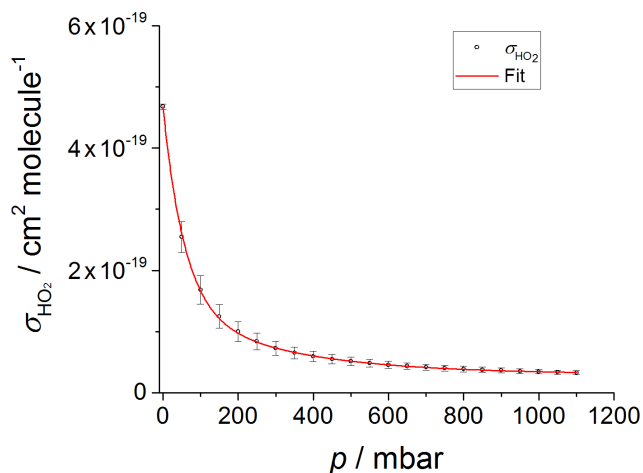
Figure 4. Absorption cross section of HO$_2$ at 1506.43 nm vs. pressure of air. The σ_{HO_2} values (circles) were computed using the line strengths of the HO$_2$ transitions contributing to the absorption at 1506.43 nm (Thiebaud et al., 2007) and the pressure broadening coefficients were assumed to be the same for all transitions and equal to the average of the values reported for the spectral region between 1499 and 1508 nm (0.115 cm^{-1} atm^{-1} = 1.14 × 10^{-4} cm^{-1} mbar^{-1}) (Ibrahim et al., 2007) as explained in the main text. The red line is a fit of Eq. (7) to the calculated values. The extracted values of the equation parameters are shown in Table S3 in the Supplement.

line and the other neighbouring HO$_2$ lines. At both pressures the minimum ring-down time, τ, occurs at 1506.43 nm. The contribution of HO$_2$ to the decrease in the ring-down time at 1506.43 nm relative to τ in the absence of reagents, $\Delta\tau$, is $\sim$ 50 % at 150 mbar and $\sim$ 20 % at 1000 mbar, with the remaining contributions due to CH$_3$OH. During the measurements, the background absorption decreased mainly due to the consumption of CH$_3$OH by the CH$_3$OH + Cl reaction (Reaction R17). [CH$_3$OH] decreased by $\sim$ 15 % during the scan at 150 mbar and $\sim$ 10 % during the scan at 1000 mbar, as determined using FTIR measurements (Supplement), to form CH$_2$O through Reaction (R17) followed by (R18). Section S7 in the Supplement shows that σ_{CH_3OH} is $\sim$ 3 times higher than σ_{CH_2O} at both pressures; hence $\sim$ 30 % of the decrease in the absorption background due to the CH$_3$OH consumption was counteracted by the formation of CH$_2$O. The spectrum was measured from larger to smaller wavelengths (right to left), hence the decrease in background absorption with time (decreasing λ) during a scan. The inset shows an example CRDS signal at 1506.43 nm and 150 mbar and the fit to the data performed by using Eq. (5) to extract τ.

$$I_t = I_0 \exp\left(-\frac{t}{\tau}\right), \tag{5}$$

where I_t is the signal detected at time t and I_0 is the signal at $t = 0$.

3.2 Determination of the absorption cross section of HO$_2$ at 1506.43 nm as a function of pressure

The absorption cross section of HO$_2$ at 1506.43 nm in the range 0–1100 mbar of air was computed by using a model which takes into account not only the feature centred at 1506.43 nm but also the contribution of the neighbouring transitions due to the air-broadening of the absorption lines. The line centres ν^* and strengths S (including the uncertainties δS) of the HO$_2$ transitions at 1506.43 nm and all the nearby transitions have been extracted from the spectra reported by Fittschen and co-workers at 50 Torr of He (Thiebaud et al., 2007). The reported absorption data were scaled so that the line strength of the main transition at 1506.43 nm becomes $S = 7.09 \times 10^{-21}$ cm^2 cm^{-1}, which we assume to be the correct value for that transition (Fittschen, personal communication, 2017). The air-broadening coefficient, γ_{air}, was assumed to be the same for all transitions, 0.115 cm^{-1} atm^{-1} = 1.14 × 10^{-4} cm^{-1} mbar^{-1} (average value of 34 HO$_2$ transitions between 6631 and 6671 cm^{-1}; Ibrahim et al., 2007). For each transition (indexed by l), an area-normalised Voigt profile $V(\nu; \nu_l^*, \Gamma_G, \Gamma_L(p))$, centred at ν_l^* (here ν and ν_l^* are wave numbers) with Gaussian width Γ_G and Lorentzian width $\Gamma_L(p)$, was computed. The absorption cross section for HO$_2$ at ν is then given by Eq. (6).

$$\sigma_{HO_2}(\nu, p) = \sum_l S_l V\left(\nu; \nu_l^*, \Gamma_G, \Gamma_L(p)\right) \tag{6}$$

In particular, the cross section for HO$_2$ at the peak location $\nu_{pk} = 6638.2$ cm^{-1} (1506.43 nm) is

$$\sigma_{HO_2} = \sigma_{HO_2}(\nu_{pk}, p) = \sum_l S_l V\left(\nu_{pk}; \nu_l^*, \Gamma_G, \Gamma_L(p)\right). \tag{7}$$

A plot of the calculated σ_{HO_2} as a function of pressure p and at 298 K is shown in Fig. 4 for pressures ranging from 0 to 1100 mbar in steps of 50 mbar. The error bars represent the uncertainties ($\pm 1\sigma$) in σ_{HO_2} arising from the uncertainties in the pressure-broadening parameter, γ_{air}, and in the line strengths, S. The error caused by γ_{air} was determined by computing σ_{HO_2}, while linearly varying γ_{air} between the minimum and maximum values reported by Fittschen and co-workers (Ibrahim et al., 2007), i.e. between 0.078 and 0.155 cm^{-1} atm^{-1}. The uncertainty caused by the error in S was determined in a similar fashion, namely by computing σ_{HO_2} while linearly varying the line strengths between $S_l - \delta S_l$ and $S_l + \delta S_l$. The simplest model that fits the simulated data is

$$\sigma_{HO_2}(\nu_{pk}, p) = A_0 + A_1 \exp(-\lambda_1 p) + A_2 \exp(-\lambda_2 p). \tag{8}$$

The values of the fit parameters, A_0, A_1, A_2, λ_1 and λ_2, are given in Table S3 in the Supplement.

The result of this work, $\sigma_{HO_2, 150\,mbar} = (1.25 \pm 0.19) \times 10^{-19}$ cm^2 molecule^{-1}, agrees very well with the value

$\sigma_{\mathrm{HO_2, 150\ mbar}} = (1.29 \pm 0.23) \times 10^{-19}$ cm^2 molecule^{-1} calculated by using the equation computed by Tang et al. (2010) to describe the change in $\sigma_{\mathrm{HO_2}}$ at 1506.43 nm and 296 K with the increase in the pressure of air observed experimentally between 27 and 133 mbar using conventional multi-pass absorption spectroscopy. $\sigma_{\mathrm{HO_2}}$ has been determined previously only at low pressures, so there is no literature value to compare with our calculated value of $\sigma_{\mathrm{HO_2, 1000\ mbar}} = (3.44 \pm 0.37) \times 10^{-20}$ cm^2 molecule^{-1}. Both $\sigma_{\mathrm{HO_2, 150\ mbar}}$ and $\sigma_{\mathrm{HO_2, 1000\ mbar}}$ were also determined by using the kinetic method to obtain [HO$_2$] presented in Sect. 3.3.

3.3 Determination of $\sigma_{\mathrm{HO_2}}$ (1506.43 nm) using the kinetics of the HO$_2$ temporal decay

3.3.1 $\sigma_{\mathrm{HO_2}}$ (1506.43 nm) at 150 mbar

The kinetics of the temporal decay of HO$_2$ monitored by CRDS when the HIRAC lamps were extinguished, i.e. the HO$_2$ absorption coefficient at 1506.43 nm ($\alpha_{\mathrm{HO_2}}$) vs. time, has been used to determine $\sigma_{\mathrm{HO_2}}$ at 150 mbar. The absorption coefficient $\alpha_{\mathrm{HO_2}}$ (the product of the absorption cross section and the concentration) was computed using Eq. (9).

$$\alpha_{\mathrm{HO_2}} = \frac{1}{c}\left(\frac{1}{\tau} - \frac{1}{\tau_0}\right), \qquad (9)$$

where c is the velocity of light and τ and τ_0 are the ring-down times recorded with the lamps on and off respectively.

The temporal decays of $\alpha_{\mathrm{HO_2}}$ were analysed to extract $\sigma_{\mathrm{HO_2}}$ in a similar fashion to how the FAGE signal decays were analysed to determine the FAGE calibration factor, $C_{\mathrm{HO_2}}$ (Eq. 4 in Sect. 2.3.2). Therefore, HO$_2$ decays were analysed using Eq. (10).

$$(\alpha_{\mathrm{HO_2}})_t = \left(\left(\frac{1}{(\alpha_{\mathrm{HO_2}})_0} + \frac{2 \cdot k_{\mathrm{self\text{-}r.}}}{k_{\mathrm{loss}} \cdot \sigma_{\mathrm{HO_2}}}\right)\right.$$
$$\left. \times \exp(k_{\mathrm{loss}}t) - \left(\frac{2 \cdot k_{\mathrm{self\text{-}r.}}}{k_{\mathrm{loss}} \cdot \sigma_{\mathrm{HO_2}}}\right)\right)^{-1}, \qquad (10)$$

where $k_{\mathrm{self\text{-}r.}}$ and k_{loss} have already been defined and $(\alpha_{\mathrm{HO_2}})_t$ and $(\alpha_{\mathrm{HO_2}})_0$ are the absorption coefficient at time t and $t = 0$ (the time when the UV lamps were switched off). Equation (10) was fitted to eight temporal traces (Fig. 5 shows an example) where the $(\alpha_{\mathrm{HO_2}})_0$ was varied by a factor of 2 to obtain an average $\sigma_{\mathrm{HO_2}} = (1.02 \pm 0.18) \times 10^{-19}$ cm^2 molecule^{-1} (see all the values in Table S4), where the error is a combination of systematic and statistical uncertainties at the 1σ level. The statistical error was only 3 %, showing that the analysis results are independent of [HO$_2$]$_0$. The obtained $\sigma_{\mathrm{HO_2}}$ is in broad agreement with the $\sigma_{\mathrm{HO_2}} = (1.25 \pm 0.19) \times 10^{-19}$ cm^2 molecule^{-1} generated by the analysis presented in Sect. 3.2. The wall loss rate coefficient, k_{loss}(CRDS) $= (0.11 \pm 0.01)$ s^{-1}, is slightly higher
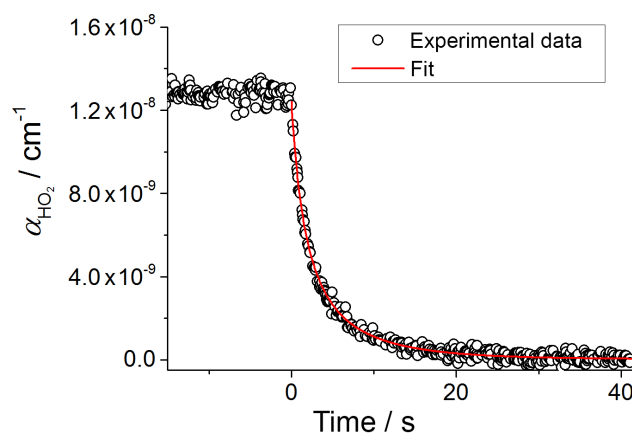
Figure 5. Second-order decay of the HO$_2$ absorption coefficient at 1506.43 nm obtained by CRDS. Experiments performed in HIRAC at 295 K and 150 mbar mixture of N$_2$:O$_2$ = 4:1; [Cl$_2$]$_0 \sim 1.5 \times 10^{14}$ molecule cm^{-3} and [CH$_3$OH]$_0 \sim 1.0 \times 10^{14}$ molecule cm^{-3}. At time zero the photolysis lamps were turned off. Fitting Eq. (10) to the data gave $\sigma_{\mathrm{HO_2}} = (1.02 \pm 0.05) \times 10^{-19}$ cm^2 molecule^{-1} (statistical error at 1σ level).

than k_{loss}(FAGE) $= (0.09 \pm 0.02)$ s^{-1}, determined by fitting the kinetic decays to calibrate the FAGE instrument. This result was expected as the FAGE instrument was measuring [HO$_2$] in the gas mixture sampled from one point at ~ 230 mm from the HIRAC wall, while CRDS measured across the total width of the chamber (1200 mm) and the two 100 mm long system of flanges coupling the cavity mirrors to the chamber (Fig. 2). The investigations into the [HO$_2$] gradient across the HIRAC diameter (86 % of the distance between the two cavity mirrors, $L = 1400$ mm) found a practically constant [HO$_2$] (Sect. 2.3.3) due to the reactive mixture homogenised by the circulation fans. As the length of the systems of flanges coupling the mirrors, where the reactive mixture might not be homogenised, represented only 14 % of L, k_{loss} was considered uniform over the entire cavity length.

Equation (9) employs the approximation that [HO$_2$] is constant along the entire length of the cavity, L. Future experiments using a flow of clean air in front of the both cavity mirrors are planned to protect them from (potential) contamination due to the reactive mixture and to test whether the results of the analysis of the HO$_2$ temporal decays remain unchanged by a virtual zero concentration of HO$_2$ in front of the mirrors. Analysis was performed considering the worst-case scenario that no HO$_2$ radicals were present over the two 100 mm distances between the cavity mirrors and the main HIRAC chamber, i.e. [HO$_2$] = 0 over 14 % of L. This analysis found the same wall loss rate coefficient on average, $k_{\mathrm{loss}} = (0.11 \pm 0.01)$ s^{-1}, as the average value obtained assuming that [HO$_2$] is constant across the entirety of L. The extracted

σ_{HO_2} $(1.18 \pm 0.22) \times 10^{-19}$ cm^2 molecule^{-1} on average has overlapping overall errors (at the 1σ level) with that found by the analysis in which [HO$_2$] was considered homogeneous along the entire L, $(1.02 \pm 0.18) \times 10^{-19}$ cm^2 molecule^{-1} (further details in Sect. S9.2 in the Supplement).

3.3.2 σ_{HO_2} (1506.43 nm) at 1000 mbar

The measured absorption coefficients $\alpha_{HO_2, 1000 \, mbar}$ were 3 times lower than $\alpha_{HO_2, 150 \, mbar}$ for the same HO$_2$ concentrations; hence the signal-to-noise ratio decreased with increasing pressure (see Figs. 5 and 6 as examples of α_{HO_2} vs. time at the two pressures). Therefore, the statistical uncertainties in the kinetic analysis of the α_{HO_2} temporal decays were relatively high at 1000 mbar, having values of 19 % in $\sigma_{HO_2, 1000 \, mbar}$ and 37 % in $k_{loss, 1000 \, mbar}$ at 1σ level on average. By comparison, the precision of the kinetic method at 1σ level at 150 mbar was 3 % in $\sigma_{HO_2, 150 \, mbar}$ and 10 % in $k_{loss, 150 \, mbar}$. In order to reduce the CRDS statistical uncertainties at 1000 mbar, the FAGE signal decays monitored at the same time with the α_{HO_2} decays were used to determine $\sigma_{HO_2, 1000 \, mbar}$. In this approach the fluorescence signal decays were scaled to overlap α_{HO_2} vs. time by multiplying the FAGE signal by $f = \frac{(\bar{\alpha}_{HO_2})_0}{(\bar{S}_{HO_2})_0}$, where $(\bar{\alpha}_{HO_2})_0$ and $(\bar{S}_{HO_2})_0$ are the mean absorption coefficient and the mean FAGE signal before the UV lamps are turned off. Equation (10), where $k_{self-r.}$ was fixed to 2.85×10^{-12} cm^3 molecule^{-1} s^{-1} (Atkinson et al., 2004), was fitted to the scaled signal decays (Fig. 6 shows an example) to obtain an average $\sigma_{HO_2} = (3.87 \pm 0.74) \times 10^{-20}$ cm^2 molecule^{-1} (further details in the Supplement), where the error limits are overall errors (19 %) quoted at the 1σ level. The value of σ_{HO_2}(FAGE) agrees very well with the average absorption cross section obtained by fitting Eq. (10) to the temporal decays recorded by the CRDS system, σ_{HO_2}(CRDS) $= (3.68 \pm 0.99) \times 10^{-20}$ cm^2 molecule^{-1} (Sect. 9.3 in the Supplement), where the overall 1σ uncertainty is 27 %. Both values are in good agreement with $\sigma_{HO_2} = (3.44 \pm 0.37) \times 10^{-20}$ cm^2 molecule^{-1} computed by the model described in Sect. 3.2, which considered the contribution of the air-broadened HO$_2$ absorption lines (Thiebaud et al., 2007) to the overall cross section at 1506.43 nm. As the precision in σ_{HO_2}(FAGE) (3 %) is much higher than the precision in σ_{HO_2}(CRDS) (19 %), σ_{HO_2}(FAGE) was used in the intercomparison of the CRDS and FAGE measurements (Sect. 3.5.2).

3.4 Determination of the CRDS detection limits

In order to quantify the sensitivity of the CRDS spectrometer, the chamber was filled with synthetic air at 150 and 1000 mbar and single ring-down events were continuously acquired at 1506.43 nm for 1.0–1.5 h. As the CRDS noise increased slightly when the fans were turned on, separate measurements were performed where the fans were main-
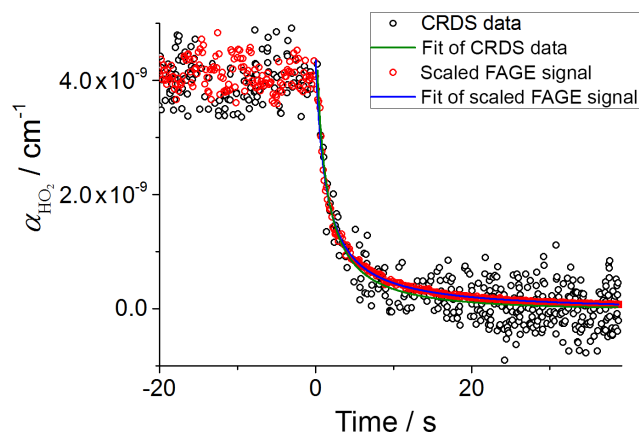
Figure 6. An example of a temporal decay of the HO$_2$ absorption coefficient at 1506.43 nm from CRDS data (black circles) along with the FAGE signal scaled to overlap the CRDS data (see text for details). The traces were recorded at 295 K and with a 1000 mbar mixture of N$_2$: O$_2$ = 4 : 1: [Cl$_2$]$_0 \sim 1.7 \times 10^{14}$ molecule cm^{-3} and [CH$_3$OH]$_0 \sim 2.0 \times 10^{14}$ molecule cm^{-3}. The fit of Eq. (10) to the CRDS data (green line) gave $\sigma_{HO_2} = (3.59 \pm 0.52) \times 10^{-20}$ cm^2 molecule^{-1}, while the fit of Eq. (10) to the scaled FAGE data (blue line) resulted in $\sigma_{HO_2} = (3.54 \pm 0.05) \times 10^{-20}$ cm^2 molecule^{-1}. The error limits are statistical errors at the 1σ level.

tained on and off. Figure S4a in the Supplement shows the separate measurements of the ring-down time at 1506.43 nm with the fans on and off as an example. The noise properties of the spectrometer can be characterised with an Allan deviation plot (Werle et al., 1993). The Allan variance, $\sigma_A^2(n)$, is the mean two-sample variance of pairs of adjacent points in a data series (absorption coefficients in our case), where each point is an average of n individual measurements (ring-down events). The Allan deviation, $\sigma_A(n)$, is $(1/\sqrt{2})$ times the root mean square value of the difference between adjacent points. As such, the Allan deviation plot (Fig. 7 and Fig. S4b in the Supplement) gives an estimate of the error, $\delta\alpha$, between successively measured absorption coefficients for a given averaging size n. At 1000 mbar, the optimum CRDS sensitivity is achieved by averaging ~ 600 ring-down events (requiring 60 s at an acquisition rate of 10 Hz), giving a minimum detectable absorption coefficient of $\delta\alpha_{min} = 2.7 \times 10^{-11}$ cm^{-1}. For n up to 3, the behaviour of $\sigma_A(n)$ is that of white noise with a bandwidth-normalised value of 1.2×10^{-10} cm^{-1} Hz$^{-1/2}$. For n up to 100, the effect of excess noise is measurable but small, and for n larger than 100 the discrepancy becomes significant. At 150 mbar, the best sensitivity of $\delta\alpha_{min} = 1.5 \times 10^{-11}$ cm^{-1} is achieved after averaging ~ 250 events (25 s). The behaviour of $\sigma_A(n)$ is that of white noise for n up to 100, with a bandwidth-normalised value of 5.8×10^{-11} cm^{-1} Hz$^{-1/2}$.

For a signal-to-noise ratio (S/N) of 2, the limits of detection for HO$_2$ were obtained from LOD$_{HO_2} = (2\delta\alpha_{min})/\sigma_{HO_2}$, and are shown in Table 1.

Table 1. CRDS detection limits for HO_2 computed at 150 and 1000 mbar for single ring-down measurements ($\Delta t = 0.1$ s), the optimum averaging time, $\Delta t_{opt.}$, 25 s at 150 mbar and 60 s at 1000 mbar and two other averaging times: $\Delta t = 3$ s and $\Delta t = 30$ s.

p_{HIRAC} / mbar	$\sigma_{HO_2} \times 10^{20}$ / cm^2 molecule^{-1}	$LOD_{HO_2} \times 10^8$ / molecule cm^{-3}			
		$\Delta t = 0.1$ s	$\Delta t = 3$ s	$\Delta t = 30$ s	$\Delta t_{opt.}$
150	12.5 ± 1.9[a]	30.4	5.6	2.7	2.4
	10.2 ± 1.8[b]	37.3	6.8	3.3	2.9
1000	3.4 ± 0.4[a]	208	44.5	16.4	15.3
	3.9 ± 0.7[b]	185	39.4	14.6	13.3

[a] Determined using the line strengths of the HO_2 transitions contributing to the absorption at 1506.43 nm (Thiebaud et al., 2007) and the pressure-broadening coefficients (Ibrahim et al., 2007) (Sect. 3.2). [b] Determined using the kinetics of the HO_2 second-order decays (Sect. 3.3).
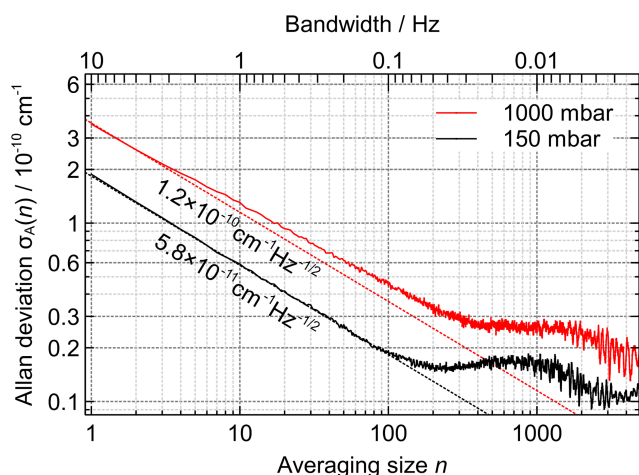
Figure 7. Allan deviation plot of the absorption coefficient at 1506.43 nm in the absence of HO_2 against the number of ring-down events averaged, n. For $S/N = 2$ the minimum detectable absorption coefficient for a single ring-down measurement is 1.9×10^{-10} cm^{-1} at 150 mbar, which is reduced to 1.5×10^{-11} cm^{-1} after averaging 250 ring-down time constants, τ_0 (requiring 25 s at an acquisition rate of 10 Hz), and 3.6×10^{-10} cm^{-1} at 1000 mbar, which decreases to 2.7×10^{-11} cm^{-1} after $n = 600$ (requiring 60 s at an acquisition rate of 10 Hz).

3.5 Intercomparison of CRDS and FAGE HO_2 measurements

3.5.1 150 mbar measurements

HO_2 was generated from photolysis of mixtures of $Cl_2/CH_3OH/O_2$ over a range of concentrations, ~ 6–750×10^8 molecule cm^{-3} at 150 mbar and ~ 4–100×10^9 molecule cm^{-3} at 1000 mbar. The comparison involved both periods with lamps on, in which $[HO_2]$ was changing slowly, and also those in which the lamps were turned off and the decay of HO_2 was followed. FAGE signals were converted into $[HO_2]$ using the calibration constant determined in Sect. 2.3.2 using the kinetic de-

cay of HO_2 ($C_{HO_2, 150 \text{ mbar}} = (2.6 \pm 0.5) \times 10^{-7}$ counts cm^3 molecule^{-1} s^{-1} mW^{-1}). CRDS absorptions were converted to concentrations based on either the cross section derived from the study of the recombination kinetics in Sect. 3.3.1 ($\sigma_{HO_2, 150 \text{ mbar}} = (1.02 \pm 0.18) \times 10^{-19}$ cm^2 molecule^{-1}) or the value of the cross section determined by application of pressure broadening to the spectral lines reported by Thiebaud et al. (2007) (Sect. 3.2; $\sigma_{HO_2, 150 \text{ mbar}} = (1.25 \pm 0.19) \times 10^{-19}$ cm^2 molecule^{-1}).

Figure 8a shows an example of a typical temporal profile of absolute HO_2 concentrations recorded over ~ 15 min first with lamps on and then with lamps switched off. The agreement between $[HO_2]$ determined by the FAGE method and the CRDS method with the cross section based on Thiebaud et al. is excellent (the difference is within 3 %). Considering errors of approximately 20 % in both the FAGE calibrations and absorption cross section determined in the kinetic studies, the FAGE-determined HO_2 concentrations are also consistent with those from CRDS with our kinetically determined absorption cross section. Figure 8b shows a correlation plot of the complete intercomparison data set with the two different absorption cross sections. The correlations are linear over the range of $[HO_2]$, ~ 6–750×10^8 molecule cm^{-3}, (average gradient $= 0.90 \pm 0.12$) with a very small negative intercept ($(-1.0 \pm 0.5) \times 10^8$ molecule cm^{-3}), which is insignificant compared to the typical HO_2 concentrations in this simulation chamber experiment.

3.5.2 1000 mbar measurements

Figure 9a and b show the equivalent comparisons for data recorded at 1000 mbar. Once again two values for the CRDS-derived concentrations are given, firstly based on the pressure-broadened cross section of Thiebaud et al. (2007) ($\sigma_{HO_2} = (3.44 \pm 0.37) \times 10^{-20}$ cm^2 molecule^{-1}) and secondly from the experimentally determined cross sections using the HO_2 decay (Sect. 3.3.2, $\sigma_{HO_2} = (3.89 \pm 0.74) \times 10^{-20}$ cm^2 molecule^{-1}). The
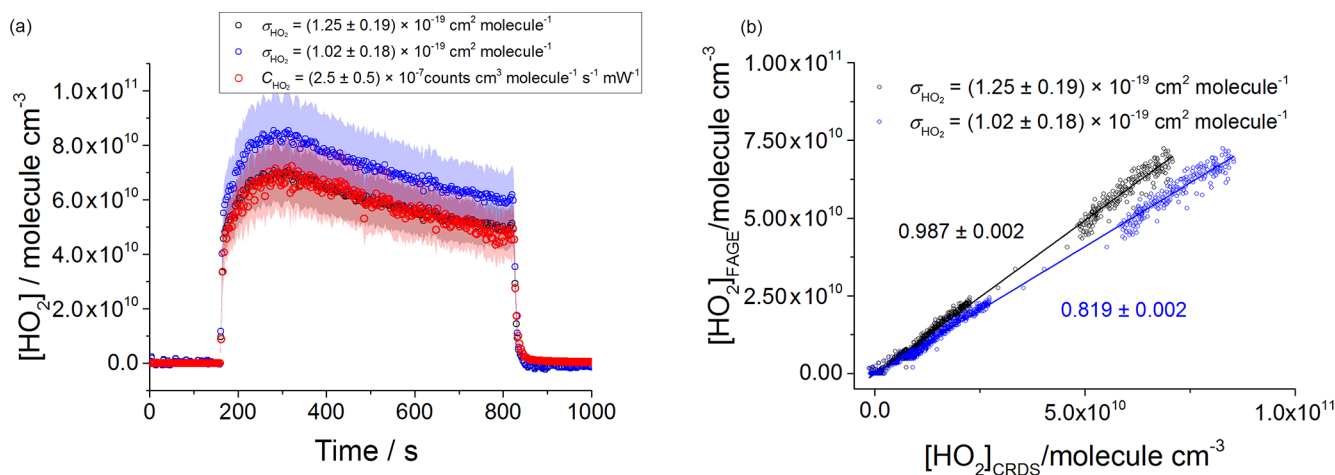
Figure 8. (a) Comparison HO$_2$ measurement at 150 mbar where the lamps were switched on at $t = \sim 150$ s for ~ 10 min. HO$_2$ measured by FAGE ($C_{150\,\text{mbar}} = 2.6 \times 10^{-7}$ counts cm^3 molecule^{-1} s^{-1} mW^{-1}, red) is plotted with HO$_2$ measured by CRDS using $\sigma_{\text{HO}_2} = 1.25 \times 10^{-19}$ cm^2 molecule^{-1} obtained (Sect. 3.2) by application of pressure broadening to the spectral lines found by Thiebaud et al. (2017) (black), and $\sigma_{\text{HO}_2} = 1.02 \times 10^{-19}$ cm^2 molecule^{-1} determined using the kinetic decays of HO$_2$ in Sect. 3.3.1 (blue). Each data point is an averaged value over 3 s. [CH$_3$OH] $= 6.6 \times 10^{13}$ molecule cm^{-3}, [Cl$_2$] $= 4.4 \times 10^{13}$ molecule cm^{-3}. **(b)** Correlation plot at 150 mbar for data plotted in **(a)**. [HO$_2$]$_\text{CRDS}$ was calculated using $\sigma_{\text{HO}_2} = 1.25 \times 10^{-19}$ cm^2 molecule^{-1} determined in Sect. 3.2 (black) and $\sigma_{\text{HO}_2} = 1.02 \times 10^{-19}$ cm^2 molecule^{-1} determined in Sect. 3.3.1 (blue). The gradients of linear unweighted fits of the data are 0.987 ± 0.002 (black) and 0.819 ± 0.002 (blue). Both lines intercept the y axis at $(-1.0 \pm 0.5) \times 10^8$ molecule cm^{-3}. [HO$_2$]$_\text{FAGE}$ was calculated using a sensitivity factor of 2.6×10^{-7} counts cm^3 molecule^{-1} s^{-1} mW^{-1} from the HO$_2$ decay as discussed in Sect. 2.3.2. Each data point is an averaged value over 3 s.

data are more scattered, reflecting the lower sensitivity of the CRDS technique at 1000 mbar, but once again the HO$_2$ concentrations determined by the two techniques (with either cross section) are consistent within the $\sim 20\%$ errors associated with the calibration of FAGE and the cross-section determinations (average gradient of the two correlation plots $= 0.84 \pm 0.08$).

4 Discussion

The HO$_2$ near-IR absorption spectrum around 1506 nm recorded in this study using CRDS is in good agreement with previous work, both in terms of the wavelength of the maximum absorption and the cross section at 150 mbar ($\sigma_{\text{HO}_2,\,150\,\text{mbar}}$), as determined here by kinetics measurements. The $\sigma_{\text{HO}_2,\,150\,\text{mbar}}$ from the kinetics studies $(1.02 \pm 0.18) \times 10^{-19}$ cm^2 molecule^{-1} (Sect. 3.3.1) is within the error ranges of the values derived from two previous studies: (i) $\sigma_{\text{HO}_2,\,150\,\text{mbar}} = (1.25 \pm 0.19) \times 10^{-19}$ cm^2 molecule^{-1} computed using the 50 mbar He measurements of Thiebaud et al. (2007), where the line centres and strengths of the HO$_2$ transitions at ~ 1506.43 nm were extracted from the reported spectra and combined with the pressure broadening in air (Ibrahim et al., 2007) (Sect. 3.2) to give σ_{HO_2} at 150 mbar, and (ii) $\sigma_{\text{HO}_2,\,150\,\text{mbar}} = (1.29 \pm 0.23) \times 10^{-19}$ cm^2 molecule^{-1} obtained by extrapolating the cross sections determined

by Tang et al. (2010) in the range of 27–133 mbar. Significant pressure broadening is observed such that the lower cross section at 1000 mbar, $\sigma_{\text{HO}_2,\,1000\,\text{mbar}}$, reducing signal to noise, makes extraction of a precise σ_{HO_2} using the CRDS data from the recombination kinetics difficult. However, a comparison of the temporal profiles of the HO$_2$ decays from CRDS and FAGE (e.g. Fig. 6) shows good agreement, and the resulting absorption cross-section, an average over the analysis of six decays, $\sigma_{\text{HO}_2} = (3.87 \pm 0.74) \times 10^{-20}$ cm^2 molecule^{-1}, is in good agreement with the value of $\sigma_{\text{HO}_2} = (3.44 \pm 0.37) \times 10^{-20}$ cm^2 molecule^{-1} obtained by the application of pressure broadening to the data of Thiebaud et al. (2007).

The good agreement (only ~ 10–15 % difference on average) between CRDS and FAGE for both the HO$_2$ concentrations with the lamps on and their temporal dependence when the lamps were switched off, as exemplified in Figs. 8 and 9 (see also Figs. S7 and S8 in the Supplement), provides validation between the absolute and direct methods of HO$_2$ detection via CRDS and the FAGE technique, which is an indirect method requiring calibration. The CRDS method requires a known σ_{HO_2} and this is not trivial to obtain for a radical species, so there are systematic uncertainties of approximately 20 % associated with CRDS measurements of HO$_2$. While no significant concerns have been raised about either the photolysis of water vapour at 185 nm in air as a
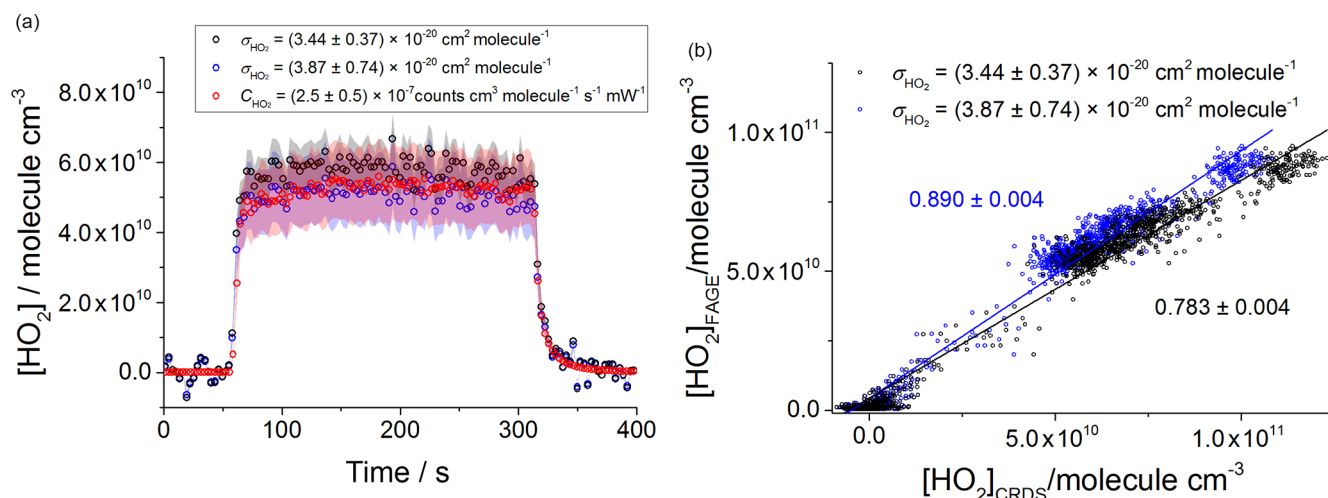
Figure 9. (a) Comparison measurement at 1000 mbar where the lamps were left on for ~ 4 min. HO$_2$ measured by FAGE using the calibration factor obtained as shown in Sect. 2.3.1: the average of the value determined by the H$_2$O photolysis and the value obtained using the HO$_2$ decays, $C_{1000\,\text{mbar}} = 2.5 \times 10^{-7}$ counts cm^3 molecule^{-1} s^{-1} mW^{-1}, red circles, is plotted with HO$_2$ measured by CRDS using $\sigma_{\text{HO}_2} = 3.44 \times 10^{-19}$ cm^2 molecule^{-1}, determined (Sect. 3.2) by application of pressure broadening to the spectral lines found by Thiebaud et al. (2017) (black circles), and $\sigma_{\text{HO}_2} = 3.87 \times 10^{-20}$ cm^2 molecule^{-1}, determined using the kinetic decays of HO$_2$ in Sect. 3.3.2 (blue circles). Each data point is an averaged value over 3 s. [CH$_3$OH] $\sim 1.65 \times 10^{15}$ molecule cm^{-3}, and [Cl$_2$] $\sim 1.10 \times 10^{14}$ molecule cm^{-3}. **(b)** Correlation plot at 1000 mbar for data in **(a)**. [HO$_2$]$_{\text{CRDS}}$ was calculated using $\sigma_{\text{HO}_2} = 3.44 \times 10^{-20}$ cm^2 determined as shown in Sect. 3.2 (black) and $\sigma_{\text{HO}_2} = 3.87 \times 10^{-20}$ cm^2 determined as shown in Sect. 3.3.2 (blue). Gradients of linear unweighted fits to the data are 0.890 ± 0.004 and 0.783 ± 0.004 and intercepts of $(-4.3 \pm 0.3) \times 10^9$ and $(-1.0 \pm 0.5) \times 10^8$ molecule cm^{-3} respectively. [HO$_2$]$_{\text{FAGE}}$ was calculated using the sensitivity factor $\bar{C}_{1000\,\text{mbar}} = 2.5 \times 10^{-7}$ counts cm^3 molecule^{-1} s^{-1} mW^{-1}, which is the average of the value determined by the H$_2$O photolysis and the mean value determined using the HO$_2$ decays (Sect. 2.3.1). Each data point is an averaged value over 3 s.

method with which to generate HO$_2$ for calibration or the indirect method of determining HO$_2$ by NO titration to OH (at least for the simple chemical environments described in this paper), this is the first direct, real time, quantitative intercomparison between CRDS and FAGE for HO$_2$ detection. The good agreement between the two techniques raises confidence for their application. Such a level of agreement provides evidence for there being no undetected systematic errors in either technique. Note that this work also supports the method used to measure HO$_2$ via the CIMS technique, as CIMS also relies on a similar methodology, namely titration with NO to convert HO$_2$ to OH (Edwards et al., 2003).

Table 2 compares the LOD of the CRDS system described here with the LOD values reported in previous studies using the first overtone of the O-H stretch in near IR to detect HO$_2$ through different techniques: CRDS (Thiebaud et al., 2007, 2008; Liu et al., 2008), noise-immune cavity-enhanced optical heterodyne molecular spectroscopy, NICE-OHMS (Bell et al., 2012) and wavelength modulation near-IR spectroscopy, WM-NIR (Noell et al., 2010). The CRDS instrument used in this work allows for more sensitive measurements of HO$_2$ than in the above-cited references. However, the instrument has insufficient sensitivity to detect ambient levels of HO$_2$, where typical maximum concentrations are very dependent upon NO$_x$ and range from (0.5–

10) $\times 10^8$ molecule cm^{-3} (Carslaw et al., 2001; Heard et al., 2004; Dusanter et al., 2009; Holland et al., 2003), and ideally a detection limit $< 1 \times 10^7$ molecule cm^{-3} is required. However, the sensitivity (LOD for [HO$_2$] with 30 s averaging at 1000 mbar $\sim 1.5 \times 10^9$ molecule cm^{-3}) is more than adequate for chamber studies, where in general [HO$_2$] $> 3 \times 10^{10}$ molecule cm^{-3} can be generated and 30 s averaging should provide good temporal resolution as experiments typically take between 10 and 120 min (Malkin et al., 2010; Winiberg et al., 2016). It is stressed, however, that the LOD quoted here is in the absence of water vapour. No change in the LOD at 150 mbar in the presence of typical ambient concentrations of water (10^{17} molecule cm^{-3} orders of magnitude) is expected at 150 mbar, as there is little overlap of the water absorption lines with the HO$_2$ absorption at 1506.43 nm at this pressure. However, in the presence of [H$_2$O] $\sim 10^{17}$ molecule cm^{-3} the CRDS sensitivity at 1000 mbar is expected to decrease markedly relative to the sensitivity in dry air found in this work due to the pressure broadening of the H$_2$O spectral lines, resulting in a significant H$_2$O absorption at 1506.43 nm in the background of the HO$_2$ measurements.

The CRDS sensitivity could be further optimised by setting up the CRDS along HIRAC to increase the cavity length to 2.0 m (from the present length of 1.4 m). Measurements of

Table 2. Comparison of the detection limits (LOD) for HO$_2$ obtained in this work with previously reported LOD (extrapolated to 30 s integration time, 0.033 Hz detection bandwidth) obtained by detecting HO$_2$ in near IR via the first vibrational overtone of the O-H stretch.

LOD / molecule cm^{-3}	Wavelength / nm	Pressure / mbar	Bath gas	Technique	Reference
$8.0 \times 10^{8,a}$	1506.43	66.7	He	CRDS	Thiebaud et al. (2007)
$5.8 \times 10^{8,b}$	1506.43	33.3	He	CRDS	Thiebaud et al. (2008)
$\sim 1 \times 10^{11,c}$	1509.27	40.0	N$_2$	CRDS	Liu et al. (2008)
$\sim 8 \times 10^{9,d}$	1509.82 and 1509.76	53.3	Ar	NICE-OHMS	Bell et al. (2012)
$\sim 1.8 \times 10^{10,e}$	1506.43	42.7–160.0	N$_2$/ O$_2$/ He	WM-NIR	Noell et al. (2010)
$3.0 \times 10^{8,f}$	1506.43	150	air	CRDS	this work
$1.5 \times 10^{9,g}$	1506.43	1000	air	CRDS	this work

^{a} Cavity ring-down spectroscopy (CRDS). Calculated for $\sigma_{HO_2} = 2.7 \times 10^{-19}$ cm^2 molecule^{-1}; $\alpha_{min} = 1.2 \times 10^{-9}$ cm^{-1} Hz$^{-1/2}$. ^{b} Calculated for $\sigma_{HO_2} = 3.4 \times 10^{-19}$ cm^2 molecule^{-1} and $\alpha_{min} = 1.1 \times 10^{-9}$ cm^{-1} Hz$^{-1/2}$. ^{c} LOD computed by using the noise level of the HO$_2$ spectrum baseline and corresponded to $\alpha_{min} \sim 3 \times 10^{-8}$ cm^{-1} for HO$_2$ generated in dielectric barrier discharge plasma; bandwidth unknown. ^{d} Noise-immune cavity-enhanced optical heterodyne molecular spectroscopy (NICE-OHMS); $\sigma_{HO_2, 1509.82} = 9.7 \times 10^{-20}$ cm^2 molecule^{-1} and $\sigma_{HO_2, 1509.76} = 1.3 \times 10^{-19}$ cm^2 molecule^{-1}; LOD calculated for a sensitivity of $\alpha_{HO_2} = 5.7 \times 10^{-9}$ cm^{-1} Hz$^{-1/2}$. ^{e} Wavelength modulation near-IR (WM-NIR) spectroscopy; LOD given as 1×10^{11} cm^{-3} Hz$^{-1/2}$; typical concentrations: $(3–15) \times 10^{16}$ molecule cm^{-3} He, $(5–20) \times 10^{17}$ molecule cm^{-3} O$_2$ and $(0–1) \times 10^{18}$ molecule cm^{-3} N$_2$. ^{f} Average of the two LOD shown in Table 1 (computed for $\sigma_{HO_2} = 1.25 \times 10^{-19}$ cm^2 molecule^{-1} and $\sigma_{HO_2} = 1.02 \times 10^{-19}$ cm^2 molecule^{-1}); $S/N = 2$. ^{g} Average of the two LOD shown in Table 1 (computed for $\sigma_{HO_2} = 3.44 \times 10^{-20}$ cm^2 molecule^{-1} and $\sigma_{HO_2} = 3.87 \times 10^{-20}$ cm^2 molecule^{-1}); $S/N = 2$.

fast kinetic decays of HO$_2$ and averaging of ring-down events where HO$_2$ is in steady-state would benefit from an increase in the frequency of the ring-down events. No improvement of the sensitivity is expected by changing the wavelength of the measurements to another value in near IR as this work has been already performed at the wavelength of the most important HO$_2$ absorption feature (1506.43 nm) in the range of $\sim$ 1493–1514 nm (vacuum wavelength corresponding to 6604–6696 cm^{-1}) where the first overtone of the O-H stretch has been observed (DeSain et al., 2003; Thiebaud et al., 2007). Even though the mid-IR range provides stronger HO$_2$ absorption cross sections (Richard et al., 2012), the near-IR region has been chosen for this study as it offers advantages such as improved performance of the detectors and optical components, which are also available at a lower cost.

In terms of practical operation, both the FAGE and CRDS methods require trained operatives and constant monitoring of conditions to ensure optimum performance: neither technique could be considered a "turn-key" process. The CRDS system does have a significant cost advantage, with the current apparatus being assembled for a cost of $\sim$ GBP 9 k.

5   Conclusions

The fluorescence assay by gas expansion (FAGE) technique is the most commonly used method for the measurement of HO$_2$ in the atmosphere by conversion of HO$_2$ to OH by reaction with added NO followed by OH on-resonance LIF at 308 nm. However, FAGE is not an absolute method and hence requires calibration. In this work an intercomparison is performed between the FAGE technique and the absolute cavity ring-down spectroscopy (CRDS) method within the Leeds HIRAC atmospheric simulation chamber. FAGE was conducted by sampling through a pinhole at $\sim$ 0.2 m from

the chamber wall (1.2 m internal diameter), while CRDS probed HO$_2$ over the entire width of the chamber, using the excitation of the first O-H overtone at 1506.43 nm. The HO$_2$ radical was generated from photolysis of mixtures of Cl$_2$/ CH$_3$OH / O$_2$ at room temperature and two total pressures (150 and 1000 mbar of synthetic air) and was monitored simultaneously using the two techniques.

At 1000 mbar FAGE was calibrated using two different methods: the conventional calibration method consisting of the 185 nm photolysis of water vapour in synthetic air and the kinetic decay of the fluorescence signal method. The two methods were in agreement to within 8 %; the average of the calibration factors obtained by the two methods was $\bar{C}_{HO_2, 1000\,mbar} = (2.5 \pm 0.5) \times 10^{-7}$ counts cm^3 molecule^{-1} s^{-1} mW^{-1}, which corresponds to a limit of detection (LOD) of 1.6×10^6 molecule cm^{-3} for a signal-to-noise (S/N) ratio of 2 and an averaging period of 30 s. At 150 mbar the kinetic method was used for FAGE calibration, which yielded $C_{HO_2} = (2.6 \pm 0.5) \times 10^{-7}$ counts cm^3 molecule^{-1} s^{-1} mW^{-1} and hence a LOD similar to that obtained at 1000 mbar. The HO$_2$ absorption cross section at 1506.43 nm, σ_{HO_2}, at 150 and 1000 mbar was determined using two independent methods: from the 50 mbar He measurements of Thiebaud et al. (2007), where the line centres and strengths of the HO$_2$ transitions at $\sim$ 1506.43 nm were extracted from the reported spectra and combined with the pressure broadening in air (Ibrahim et al., 2007), and from the kinetics of the second-order HO$_2$ decays. At each operating pressure the values of σ_{HO_2} obtained by the two methods agree with each other (within $\sim$ 12 % agreement at 1000 mbar and within $\sim$ 20 % agreement at 150 mbar). For a time resolution of 30 s the computed CRDS sensitivity using the Allan deviation

plots and the average σ_{HO_2} at each pressure are 3.0×10^8 at 150 mbar and 1.5×10^9 molecule cm^{-3} at 1000 mbar.

The comparison was performed both for periods in which [HO$_2$] was decreasing slowly for 5–10 min and periods in which the lamps were shortly turned on and then off to generate a series of HO$_2$ decays to encompass a wide range of [HO$_2$]: ~ 6–750×10^8 molecule cm^{-3} at 150 mbar and ~ 4–100×10^9 molecule cm^{-3} at 1000 mbar. The correlation plots at both pressures show a good agreement between [HO$_2$] measured using the indirect FAGE method and the direct CRDS method: a gradient of 0.987 ± 0.002 when σ_{HO_2} determined by application of pressure broadening to the reported spectral lines (Thiebaud et al., 2007) was used at 150 mbar and average gradients (of the results obtained using the two σ_{HO_2} values at each pressure) of 0.90 ± 0.12 at 150 mbar and of 0.84 ± 0.08 at 1000 mbar. This intercomparison study provides validation for the FAGE method and supports the use of the method employing CIMS for HO$_2$ measurements, which also relies on the conversion of HO$_2$ to OH by titration with NO (Edwards et al., 2003).

Competing interests. The authors declare that they have no conflict of interest.

The Supplement related to this article is available online at https://doi.org/10.5194/amt-10-4877-2017-supplement.

Edited by: Hendrik Fuchs
Reviewed by: two anonymous referees

References

Assaf, E., Asvany, O., Votava, O., Batut, S., Schoemaecker, C., and Fittschen, C.: Measurement of line strengths in the $\widetilde{A}^2$A' $\leftarrow \widetilde{X}^{\sim 2}$ A transition of HO$_2$ and DO$_2$, J. Quant. Spectrosc. Ra., 201, 161–170, https://doi.org/10.1016/j.jqsrt.2017.07.004, 2017.

Atkinson, R., Baulch, D. L., Cox, R. A., Crowley, J. N., Hampson, R. F., Hynes, R. G., Jenkin, M. E., Rossi, M. J., and Troe, J.: Evaluated kinetic and photochemical data for atmospheric chemistry: Volume I – gas phase reactions of O$_x$, HO$_x$, NO$_x$ and SO$_x$ species, Atmos. Chem. Phys., 4, 1461–1738, https://doi.org/10.5194/acp-4-1461-2004, 2004.

Bell, C. L., van Helden, J. P. H., Blaikie, T. P. J., Hancock, G., van Leeuwen, N. J., Peverall, R., and Ritchie, G. A. D.: Noise-Immune Cavity-Enhanced Optical Heterodyne Detection of HO$_2$ in the Near-Infrared Range, J. Phys. Chem. A, 116, 5090–5099, https://doi.org/10.1021/jp301038r, 2012.

Blin-Simiand, N., Pasquiers, S., and Magne, L.: Removal of formaldehyde by a pulsed dielectric barrier discharge in dry air in the 20 °C to 300 °C temperature range, J. Phys. D. Appl. Phys., 49, 195202, https://doi.org/10.1088/0022-3727/49/19/195202, 2016.

Blocquet, M., Schoemaecker, C., Amedro, D., Herbinet, O., Battin-Leclerc, F., and Fittschen, C.: Quantification of OH and HO$_2$ radicals during the low-temperature oxidation of hydrocarbons by Fluorescence Assay by Gas Expansion technique, P. Natl. Acad. Sci. USA, 110, 20014–20017, https://doi.org/10.1073/pnas.1314968110, 2013.

Bloss, W. J., Lee, J. D., Johnson, G. P., Sommariva, R., Heard, D. E., Saiz-Lopez, A., Plane, J. M. C., McFiggans, G., Coe, H., Flynn, M., Williams, P., Rickard, A. R., and Fleming, Z. L.: Impact of halogen monoxide chemistry upon boundary layer OH and HO$_2$ concentrations at a coastal site, Geophys. Res. Lett., 32, L06814, https://doi.org/10.1029/2004gl022084, 2005.

Brown, S. S.: Absorption spectroscopy in high-finesse cavities for atmospheric studies, Chem. Rev., 103, 5219–5238, https://doi.org/10.1021/cr020645c, 2003.

Brumfield, B., Sun, W. T., Ju, Y. G., and Wysocki, G.: Direct In Situ Quantification of HO$_2$ from a Flow Reactor, J. Phys. Chem. Lett., 4, 872–876, https://doi.org/10.1021/jz400143c, 2013.

Cantrell, C. A. and Stedman, D. H.: A possible technique for the measurement of atmospheric peroxy-radicals, Geophys. Res. Lett., 9, 846–849, https://doi.org/10.1029/GL009i008p00846, 1982.

Cantrell, C. A., Stedman, D. H., and Wendel, G. J.: Measurement of atmospheric peroxy-radicals by chemical amplification, Anal. Chem., 56, 1496–1502, https://doi.org/10.1021/ac00272a065, 1984.

Carslaw, N., Creasey, D. J., Harrison, D., Heard, D. E., Hunter, M. C., Jacobs, P. J., Jenkin, M. E., Lee, J. D., Lewis, A. C., Pilling, M. J., Saunders, S. M., and Seakins, P. W.: OH and HO$_2$ radical chemistry in a forested region of north-western Greece, Atmos. Environ., 35, 4725–4737, 2001.

Chen, D. X., Huey, L. G., Tanner, D. J., Li, J. F., Ng, N. L., and Wang, Y. H.: Derivation of Hydroperoxyl Radical Levels at an Urban Site via Measurement of Pernitric Acid by Iodide Chemical Ionization Mass Spectrometry, Environ. Sci. Technol., 51, 3355–3363, https://doi.org/10.1021/acs.est.6b05169, 2017.

Chen, Y., Yang, C., Zhao, W., Fang, B., Xu, X., Gai, Y., Lin, X., Chen, W., and Zhang, W.: Ultra-sensitive measurement of peroxy radicals by chemical amplification broad-band cavity-enhanced spectroscopy, Analyst, 141, 5870–5878, https://doi.org/10.1039/c6an01038e, 2016.

Christensen, L. E., Okumura, M., Sander, S. P., Friedl, R. R., Miller, C. E., and Sloan, J. J.: Measurements of the rate constant of HO$_2$ + NO$_2$ = HO$_2$NO$_2$ using near-infrared wavelength-modulation spectroscopy and UV-visible

absorption spectroscopy, J. Phys. Chem. A, 108, 80–91, https://doi.org/10.1021/jp035905o, 2004.

DeSain, J. D., Ho, A. D., and Taatjes, C. A.: High-resolution diode laser absorption spectroscopy of the O-H stretch overtone band $(2,0,0) \leftarrow (0,0,0)$ of the HO$_2$ radical, J. Mol. Spectrosc., 219, 163–169, 10.1016/s0022-2852(03)00022-5, 2003.

Djehiche, M., Tomas, A., Fittschen, C., and Coddeville, P.: First Cavity Ring-Down Spectroscopy HO$_2$ Measurements in a Large Photoreactor, Z. Phys. Chem., 225, 983–992, https://doi.org/10.1524/zpch.2011.0143, 2011.

Djehiche, M., Tan, N. L. L., Jain, C. D., Dayma, G., Dagaut, P., Chauveau, C., Pillier, L., and Tomas, A.: Quantitative Measurements of HO$_2$ and Other Products of n-Butane Oxidation (H$_2$O$_2$, H$_2$O, CH$_2$O, and C$_2$H$_4$) at Elevated Temperatures by Direct Coupling of a Jet-Stirred Reactor with Sampling Nozzle and Cavity Ring-Down Spectroscopy (cw-CRDS), J. Am. Chem. Soc., 136, 16689–16694, https://doi.org/10.1021/ja510719k, 2014.

Dusanter, S., Vimal, D., Stevens, P. S., Volkamer, R., and Molina, L. T.: Measurements of OH and HO$_2$ concentrations during the MCMA-2006 field campaign – Part 1: Deployment of the Indiana University laser-induced fluorescence instrument, Atmos. Chem. Phys., 9, 1665–1685, https://doi.org/10.5194/acp-9-1665-2009, 2009.

Edwards, G. D., Cantrell, C. A., Stephens, S., Hill, B., Goyea, O., Shetter, R. E., Mauldin, R. L., Kosciuch, E., Tanner, D. J., and Eisele, F. L.: Chemical ionization mass spectrometer instrument for the measurement of tropospheric HO$_2$ and RO$_2$, Anal. Chem., 75, 5317–5327, https://doi.org/10.1021/ac034402b, 2003.

Fuchs, H., Holland, F., and Hofzumahaus, A.: Measurement of tropospheric RO$_2$ and HO$_2$ radicals by a laser-induced fluorescence instrument, Rev. Sci. Instrum., 79, 084104, https://doi.org/10.1063/1.2968712, 2008.

Fuchs, H., Brauers, T., Häseler, R., Holland, F., Mihelcic, D., Müsgen, P., Rohrer, F., Wegener, R., and Hofzumahaus, A.: Intercomparison of peroxy radical measurements obtained at atmospheric conditions by laser-induced fluorescence and electron spin resonance spectroscopy, Atmos. Meas. Tech., 2, 55–64, https://doi.org/10.5194/amt-2-55-2009, 2009.

Fuchs, H., Brauers, T., Dorn, H.-P., Harder, H., Häseler, R., Hofzumahaus, A., Holland, F., Kanaya, Y., Kajii, Y., Kubistin, D., Lou, S., Martinez, M., Miyamoto, K., Nishida, S., Rudolf, M., Schlosser, E., Wahner, A., Yoshino, A., and Schurath, U.: Technical Note: Formal blind intercomparison of HO$_2$ measurements in the atmosphere simulation chamber SAPHIR during the HOxComp campaign, Atmos. Chem. Phys., 10, 12233–12250, https://doi.org/10.5194/acp-10-12233-2010, 2010.

Fuchs, H., Bohn, B., Hofzumahaus, A., Holland, F., Lu, K. D., Nehr, S., Rohrer, F., and Wahner, A.: Detection of HO$_2$ by laser-induced fluorescence: calibration and interferences from RO$_2$ radicals, Atmos. Meas. Tech., 4, 1209–1225, https://doi.org/10.5194/amt-4-1209-2011, 2011.

Gianella, M., Reuter, S., Aguila, A. L., Ritchie, G. A. D., and van Helden, J. P. H.: Detection of HO$_2$ in an atmospheric pressure plasma jet using optical feedback cavity-enhanced absorption spectroscopy, New J. Phys., 18, 113027, https://doi.org/10.1088/1367-2630/18/11/113027, 2016.

Glowacki, D. R., Goddard, A., Hemavibool, K., Malkin, T. L., Commane, R., Anderson, F., Bloss, W. J., Heard, D. E., Ingham, T., Pilling, M. J., and Seakins, P. W.: Design of and initial results from a Highly Instrumented Reactor for Atmospheric Chemistry (HIRAC), Atmos. Chem. Phys., 7, 5371–5390, https://doi.org/10.5194/acp-7-5371-2007, 2007.

Green, T. J., Reeves, C. E., Fleming, Z. L., Brough, N., Rickard, A. R., Bandy, B. J., Monks, P. S., and Penkett, S. A.: An improved dual channel PERCA instrument for atmospheric measurements of peroxy radicals, J. Environ. Monitor., 8, 530–536, https://doi.org/10.1039/b514630e, 2006.

Hanke, M., Uecker, J., Reiner, T., and Arnold, F.: Atmospheric peroxy radicals: ROXMAS, a new mass-spectrometric methodology for speciated measurements of HO$_2$ and ΣRO$_2$ and first results, Int. J. Mass Spectrom., 213, 91–99, https://doi.org/10.1016/s1387-3806(01)00548-6, 2002.

Hard, T. M., Chan, C. Y., Mehrabzadeh, A. A., and Obrien, R. J.: Diurnal HO$_2$ Cycles at Clean-air and Urban Sites in the Troposphere, J. Geophys. Res.-Atmos., 97, 9785–9794, 1992.

Heard, D. E. and Pilling, M. J.: Measurement of OH and HO$_2$ in the troposphere, Chem. Rev., 103, 5163–5198, https://doi.org/10.1021/cr020522s, 2003.

Heard, D. E., Carpenter, L. J., Creasey, D. J., Hopkins, J. R., Lee, J. D., Lewis, A. C., Pilling, M. J., Seakins, P. W., Carslaw, N., and Emmerson, K. M.: High levels of the hydroxyl radical in the winter urban troposphere, Geophys. Res. Lett., 31, L18112, https://doi.org/10.1029/2004GL020544, 2004.

Holland, F., Hofzumahaus, A., Schafer, R., Kraus, A., and Patz, H. W.: Measurements of OH and HO$_2$ radical concentrations and photolysis frequencies during BERLIOZ, J. Geophys. Res.-Atmos., 108, 8246, https://doi.org/10.1029/2001jd001393, 2003.

Ibrahim, N., Thiebaud, J., Orphal, J., and Fittschen, C.: Air-broadening coefficients of the HO$_2$ radical in the $2\nu_1$ band measured using cw-CRDS, J. Mol. Spectrosc., 242, 64–69, https://doi.org/10.1016/j.jms.2007.02.007, 2007.

Kircher, C. C. and Sander, S. P.: Kinetics and mechanism of HO$_2$ and DO$_2$ disproportionations, J. Phys. Chem.-US, 88, 2082–2091, https://doi.org/10.1021/j150654a029, 1984.

Kurimoto, N., Brumfield, B., Yang, X. L., Wada, T., Dievart, P., Wysocki, G., and Ju, Y. G.: Quantitative measurements of HO$_2$/H$_2$O$_2$ and intermediate species in low and intermediate temperature oxidation of dimethyl ether, P. Combust. Inst., 35, 457–464, https://doi.org/10.1016/j.proci.2014.05.120, 2015.

Levy, H.: Normal Atmosphere – Large Radical and Formaldehyde Concentrations Predicted, Science, 173, 141–143, https://doi.org/10.1126/science.173.3992.141, 1971.

Liu, Z. W., Xu, Y., Yang, X. F., Zhu, A. M., Zhao, G. L., and Wang, W. G.: Determination of the HO$_2$ radical in dielectric barrier discharge plasmas using near-infrared cavity ring-down spectroscopy, J. Phys. D. Appl. Phys., 41, 045203, https://doi.org/10.1088/0022-3727/41/4/045203, 2008.

Lu, K. D., Rohrer, F., Holland, F., Fuchs, H., Bohn, B., Brauers, T., Chang, C. C., Häseler, R., Hu, M., Kita, K., Kondo, Y., Li, X., Lou, S. R., Nehr, S., Shao, M., Zeng, L. M., Wahner, A., Zhang, Y. H., and Hofzumahaus, A.: Observation and modelling of OH and HO$_2$ concentrations in the Pearl River Delta 2006: a missing OH source in a VOC rich atmosphere, Atmos. Chem. Phys., 12, 1541–1569, https://doi.org/10.5194/acp-12-1541-2012, 2012.

Malkin, T. L., Goddard, A., Heard, D. E., and Seakins, P. W.: Measurements of OH and HO$_2$ yields from the gas phase ozonolysis of isoprene, Atmos. Chem. Phys., 10, 1441–1459, https://doi.org/10.5194/acp-10-1441-2010, 2010.

Mihelcic, D., Ehhalt, D. H., Klomfass, J., Kulessa, G. F., Schmidt, U., and Trainer, M.: Measurements of free-radicals in atmosphere by matrix-isolation and electron-paramagnetic resonance, Ber. Bunsen Phys. Chem., 82, 16–19, 1978.

Miyazaki, K., Parker, A. E., Fittschen, C., Monks, P. S., and Kajii, Y.: A new technique for the selective measurement of atmospheric peroxy radical concentrations of HO$_2$ and RO$_2$ using a denuding method, Atmos. Meas. Tech., 3, 1547–1554, https://doi.org/10.5194/amt-3-1547-2010, 2010.

Morajkar, P., Schoemaecker, C., Okumura, M., and Fittschen, C.: Direct Measurement of the Equilibrium Constants of the Reaction of Formaldehyde and Acetaldehyde with HO$_2$ Radicals, Int. J. Chem. Kinet., 46, 245–259, https://doi.org/10.1002/kin.20817, 2014.

Noell, A. C., Alconcel, L. S., Robichaud, D. J., Okumura, M., and Sander, S. P.: Near-Infrared Kinetic Spectroscopy of the HO$_2$ and C$_2$H$_5$O$_2$ Self-Reactions and Cross Reactions, J. Phys. Chem. A, 114, 6983–6995, https://doi.org/10.1021/jp912129j, 2010.

O'Keefe, A. and Deacon, D. A. G.: Cavity Ring-Down Optical Spectrometer for Absorption-measurements Using Pulsed Laser Sources, Rev. Sci. Instrum., 59, 2544–2551, 1988.

Onel, L., Brennan, A., Seakins, P. W., Whalley, L., and Heard, D. E.: A new method for atmospheric detection of the CH$_3$O$_2$ radical, Atmos. Meas. Tech., 10, 3985–4000, https://doi.org/10.5194/amt-10-3985-2017, 2017.

Parker, A. E., Jain, C., Schoemaecker, C., Szriftgiser, P., Votava, O., and Fittschen, C.: Simultaneous, time-resolved measurements of OH and HO$_2$ radicals by coupling of high repetition rate LIF and cw-CRDS techniques to a laser photolysis reactor and its application to the photolysis of H$_2$O$_2$, Appl. Phys. B-Lasers O., 103, 725–733, https://doi.org/10.1007/s00340-010-4225-1, 2011.

Ren, X. R., Edwards, G. D., Cantrell, C. A., Lesher, R. L., Metcalf, A. R., Shirley, T., and Brune, W. H.: Intercomparison of peroxy radical measurements at a rural site using laser-induced fluorescence and Peroxy Radical Chemical Ionization Mass Spectrometer (PerCIMS) techniques, J. Geophys. Res.-Atmos., 108, 4605, https://doi.org/10.1029/2003jd003644, 2003.

Richard, C., Gordon, I. E., Rothman, L. S., Abel, M., Frommhold, L., Gustafsson, M., Hartmann, J. M., Hermans, C., Lafferty, W. J., Orton, G. S., Smith, K. M., and Tran, H.: New section of the HITRAN database: Collision-induced absorption (CIA), J. Quant. Spectrosc. Ra., 113, 1276–1285, https://doi.org/10.1016/j.jqsrt.2011.11.004, 2012.

Sanchez, J., Tanner, D. J., Chen, D., Huey, L. G., and Ng, N. L.: A new technique for the direct detection of HO$_2$ radicals using bromide chemical ionization mass spectrometry (Br-CIMS): initial characterization, Atmos. Meas. Tech., 9, 3851–3861, https://doi.org/10.5194/amt-9-3851-2016, 2016.

Schocker, A., Uetake, M., Kanno, N., Koshi, M., and Tonokura, K.: Kinetics and rate constants of the reaction CH$_2$OH + O$_2$ → CH$_2$O + HO$_2$ in the temperature range of 236–600 K, J. Phys. Chem. A, 111, 6622–6627, https://doi.org/10.1021/jp0682513, 2007.

Stone, D., Whalley, L. K., and Heard, D. E.: Tropospheric OH and HO$_2$ radicals: field measurements and

model comparisons, Chem. Soc. Rev., 41, 6348–6404, https://doi.org/10.1039/c2cs35140d, 2012.

Taatjes, C. A. and Oh, D. B.: Time-resolved wavelength modulation spectroscopy measurements of HO$_2$ kinetics, Appl. Optics, 36, 5817–5821, https://doi.org/10.1364/ao.36.005817, 1997.

Tang, Y. X., Tyndall, G. S., and Orlando, J. J.: Spectroscopic and Kinetic Properties of HO$_2$ Radicals and the Enhancement of the HO$_2$ Self Reaction by CH$_3$OH and H$_2$O, J. Phys. Chem. A, 114, 369–378, https://doi.org/10.1021/jp905279b, 2010.

Thiebaud, J. and Fittschen, C.: Near infrared cw-CRDS coupled to laser photolysis: Spectroscopy and kinetics of the HO$_2$ radical, Appl. Phys. B-Lasers O., 85, 383–389, https://doi.org/10.1007/s00340-006-2304-0, 2006.

Thiebaud, J., Crunaire, S., and Fittschen, C.: Measurements of line strengths in the 2 ν_1 band of the HO$_2$ radical using laser photolysis/continuous wave cavity ring-down spectroscopy (cw-CRDS), J. Phys. Chem. A, 111, 6959–6966, https://doi.org/10.1021/jp0703307, 2007.

Thiebaud, J., Parker, A., Fittschen, C., Vincent, G., Zahraa, O., and Marquaire, P. M.: Detection of HO$_2$ radicals in the photocatalytic oxidation of methyl ethyl ketone, J. Phys. Chem. C, 112, 2239–2243, https://doi.org/10.1021/jp711388k, 2008.

Werle, P., Mucke, R., and Slemr, F.: The limits of signal averaging in atmospheric trace-gas monitoring by Tunable Diode-Laser Absorption Spectroscopy (TDLAS), Appl. Phys. B-Photo., 57, 131–139, https://doi.org/10.1007/bf00425997, 1993.

Whalley, L. K., Blitz, M. A., Desservettaz, M., Seakins, P. W., and Heard, D. E.: Reporting the sensitivity of laser-induced fluorescence instruments used for HO$_2$ detection to an interference from RO$_2$ radicals and introducing a novel approach that enables HO$_2$ and certain RO$_2$ types to be selectively measured, Atmos. Meas. Tech., 6, 3425–3440, https://doi.org/10.5194/amt-6-3425-2013, 2013.

Wheeler, M. D., Newman, S. M., Orr-Ewing, A. J., and Ashfold, M. N. R.: Cavity ring-down spectroscopy, J. Chem. Soc. Faraday T., 94, 337–351, 1998.

Winiberg, F. A. F., Smith, S. C., Bejan, I., Brumby, C. A., Ingham, T., Malkin, T. L., Orr, S. C., Heard, D. E., and Seakins, P. W.: Pressure-dependent calibration of the OH and HO$_2$ channels of a FAGE HO$_x$ instrument using the Highly Instrumented Reactor for Atmospheric Chemistry (HIRAC), Atmos. Meas. Tech., 8, 523–540, https://doi.org/10.5194/amt-8-523-2015, 2015.

Winiberg, F. A. F., Dillon, T. J., Orr, S. C., Groß, C. B. M., Bejan, I., Brumby, C. A., Evans, M. J., Smith, S. C., Heard, D. E., and Seakins, P. W.: Direct measurements of OH and other product yields from the HO$_2$ + CH$_3$C(O)O$_2$ reaction, Atmos. Chem. Phys., 16, 4023–4042, https://doi.org/10.5194/acp-16-4023-2016, 2016.

Yamada, C., Endo, Y., and Hirota, E.: Difference frequency laser spectroscopy of the ν1 band of the HO$_2$ radical, J. Chem. Phys., 78, 4379–4384, https://doi.org/10.1063/1.445321, 1983.

Zador, J., Taatjes, C. A., and Fernandes, R. X.: Kinetics of elementary reactions in low-temperature autoignition chemistry, Prog. Energ. Combust., 37, 371–421, https://doi.org/10.1016/j.pecs.2010.06.006, 2011.

Zahniser, M. S. and Stanton, A. C.: A measurement of the vibrational band strength for the ν3 band of the HO$_2$ radical, J. Chem. Phys., 80, 4951–4960, https://doi.org/10.1063/1.446517, 1984.